Title	Studies on Catalytic Hydrogenation of Carbon Dioxide to Hydrocarbons
Author(s)	安藤, 尚功
Citation	大阪大学, 2000, 博士論文
Version Type	VoR
URL	https://doi.org/10.11501/3172724
rights	
Note	

Studies on Catalytic Hydrogenation of Carbon Dioxide to Hydrocarbons

（二酸化炭素の接触水素化による炭化水素合成に関する研究）

Hisanori ANDO
（安藤 尚功）

Osaka National Research Institute, AIST
（大阪工業技術研究所）

2000

Studies on Catalytic Hydrogenation of

Carbon Dioxide to Hydrocarbons

Hisanori ANDO

Osaka National Research Institute, AIST

2000

Preface

The work of this thesis has been performed under the guidance of Dr. Yoshie SOUMA at Osaka National Research Institute, AIST (ONRI). The author deeply appreciates her helpful guidance, suggestion and encouragement throughout this work.

The author wishes to make a grateful acknowledgment to Professor Shozo YANAGIDA (Faculty of Engineering, Osaka University), Professor Masakatsu NOMURA (Faculty of Engineering, Osaka University) and Professor Shun-ichi FUKUZUMI (Faculty of Engineering, Osaka University) for their helpful suggestions and stimulating discussions. The author wishes to express his sincerest acknowledgment to Dr. Yasuyuki MATSUMURA (ONRI) for his help on many stages in the preparation of papers.

The author is grateful to Dr. Mutsuo TANAKA (ONRI) for his appropriate advice and support at any time. The author should express his gratitude to Dr. Yoshiko NAKAHARA (Research Institute of Innovative Technology for the Earth; RITE), Dr. Tetsuhiko KOBAYASHI (ONRI) and Dr. Masahiro FUJIWARA (ONRI) for their invaluable assistance. The author's thanks are also given to all member of Synthetic Chemistry Section for their kindness. The author is deeply indebted to Ms. Midori SHIMADA and Ms. Keiko YANASHIMA for their assistance. They must be the best secretaries in the world.

Finally, the author would like to express his thanks to his wife Hitomi for her hearty encouragement and understanding.

Ikeda, Osaka

January 2000
Hisanori ANDO

List of Publications

1. Methanation of carbon dioxide over $LaNi_4X$-type intermetallic compounds as catalyst precursor

   Ando, H.; Fujiwara, M.; Matsumura, Y.; Miyamura, H.; Tanaka, H.; Souma, Y.
   Journal of Alloys and Compounds, **223**, 139(1995).

2. Methanation of carbon dioxide over $LaNi_4X$ type catalysts

   Ando, H.; Fujiwara, M.; Matsumura, Y.; Miyamura, H.; Souma, Y.
   Energy Conversion and Management, **36**, 653(1995).

3. Catalytic hydrogenation of carbon dioxide over $LaNi_5$ activated during the reaction

   Ando, H.; Fujiwara, M.; Matsumura, Y.; Tanaka, M.; Souma, Y.
   Journal of Molecular Catalysis A:Chemical, **114**(1), 117(1999).

4. Hydrocarbon synthesis from CO_2 over Fe-Cu catalysts

   Ando, H.; Xu, Q.; Fujiwara, M.; Matsumura, Y.; Tanaka, M.; Soumam Y.
   Catalysis Today, **45**(1-4), 229(1998).

5. A comparative study of hydrogenation of carbon dioxide and carbon monoxide over iron catalyst

   Ando, H.; Matsumura, Y.; Souma, Y.
   Journal of Molelcular Catalysis A:Chemical., *in press*.

6. Active phase of iron catalyst for alcohol formation in hydrogenation of carbon oxides

   Ando, H.; Matsumura, Y.; Souma, Y.
   Applied Organometallic Chemistry, accepted.

Contents

3.2. Comparative study of the hydrogenation of CO_x over Fe catalyst

Introduction

General Introduction

Global warming is one of the most serious problems among the recent environmental issues in the world. The global warming is caused by the accumulation of greenhouse effect gases, such as carbon dioxide (CO_2), methane (CH_4), nitrous oxide (N_2O) and halogenated hydrocarbons (CFCs) [1]. Among these gases, CO_2 is believed to have the highest contribution to the global warming, so many scientists have been investigating to reduce the concentration of CO_2 in the globe [1]. Since CO_2 is the final oxidation product of organic compounds, the large amount of additional energy is necessary for the transformation of CO_2. Consequently, most of scientists considered that the catalytic hydrogenation of CO_2 makes nonsense if the final aim of the research is the mitigation of CO_2 in the atmosphere.

Formic acid   MeOH

CO_2 ⟶ Hydrocarbons

Alcohols   CO
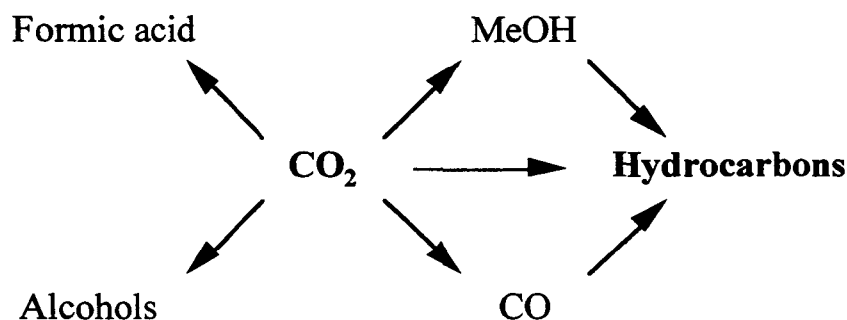
Scheme. Conversion of CO_2 by catalytic hydrogenation.

On the other hand, all living things utilize CO_2 as an ultimate carbon resource. Fossil fuels, such as petroleum oil, coal, and natural gas, are the fruits originated from the assimilation of CO_2 by plants. From these view points, the artificial utilization of CO_2 as carbon resource must be a quite interesting and important subject. If CO_2 is transformed into CO, the chemistry of CO can be applicable that has been thoroughly investigated for long time. Then the most of studies for utilization of CO_2 are focused on the syntheses of aliphatic or aromatic hydrocarbons and oxygenates such as alcohols by means of the catalytic hydrogenation as well as CO hydrogenation (see Scheme).

1

However, it is known that the catalytic performance of the catalysts for CO hydrogenation was significantly low when they were subjected to the reaction of CO_2 [2, 3]. The most important process of the conversion of CO_2 to hydrocarbons seems to be the hydrogenation of CO_2 to CO (reverse water-gas shift reaction). The surface status of the catalyst is significantly changed by water produced during the process and this change is the fatal drawback to the CO_2 transformation [4].

The final goal of this thesis is to establish a new concept to develop the highly active catalysts for the transformation of CO_2 into hydrocarbons.

In Chapter 1, the catalytic activity of a series of hydrogen storage alloys mainly containing lanthanum and nickel has been studied in order to find the effective catalyst species for the reduction of CO_2 and also to examine the relation of hydrogen storage ability with the catalysis.

Chapter 2 deals with the hydrogenation of CO_2 over Fe-based catalysts. In section 2.1, the reaction of CO_2 over copper-promoted iron catalysts has been investigated to clarify the active phase for the olefin formation. In section 2.2, the hydrogenations of CO and CO_2 over Fe catalyst were carried out and their catalytic activities were compared. Steam was added to the reactant gas mixture to examine the effect of H_2O on the catalytic activity as well as to clarify the change in the surface phase of the catalyst.

In Chapter 3, characterization of the catalyst for the hydrogenations of CO and CO_2 has been carried out. In section 3.1, the phase transformation of $LaNi_5$ during the reaction has been traced and the interaction between nickel and lanthanum is discussed. In section 3.2, the activation processes in the hydrogenation of CO and CO_2 over iron catalysts have been compared and the active sites of the reactions with CO and CO_2 have been characterized.

References

[1] V. Ramanathan, *J. Geophys. Res.*, **90**, 5547 (1985).

[2] D. J. Dwyer, G. A. Somorjai, *J. Catal.*, **52**, 291 (1978).

[3] J.-F. Lee, W.-S. Chern, M.-D. Lee, T.-Y. Dong, *Can. J. Chem. Eng.*, **70**, 511 (1992).

[4] K. Fujimoto, T. Shikada, *Appl. Catal.*, **31**, 13 (1987).

Chapter 1

Methanation of Carbon Dioxide over LaNi4X Type Intermetallic Compounds as Catalyst Precursor

1.1. Introduction

Since hydrogen storage alloys are expected to activate hydrogen, they have often been employed as catalysts for the hydrogenation of unsaturated compounds, such as ethylene, propene, 1-undecene and 2-methyl-1,3-butadiene [1-4]. The alloys also catalyze the hydrogenation of carbon monoxide to methane [5-7]. However, the alloys previously reported as hydrogenation catalysts for carbon monoxide were perfectly decomposed under the reaction conditions and lost their hydrogen storage ability. Thus, the catalytic activity should be due to metallic aggregations generated from the alloys, while the activity of hydrogen storage alloy itself has not been clarified [8,9].

In this chapter, we have studied the catalytic activity of a series of hydrogen storage alloys mainly containing lanthanum and nickel to find the effective catalyst species for the reduction of carbon dioxide known as a global warming gas and also to examine the contribution of hydrogen storage ability to the catalysis.

1.2. Experimental

The intermetallic compounds $LaNi_4X$ (X = Ni, Cr, Al, Cu) were prepared by arc-melting metal constituents in a copper crucible under 66.7 kPa argon

3
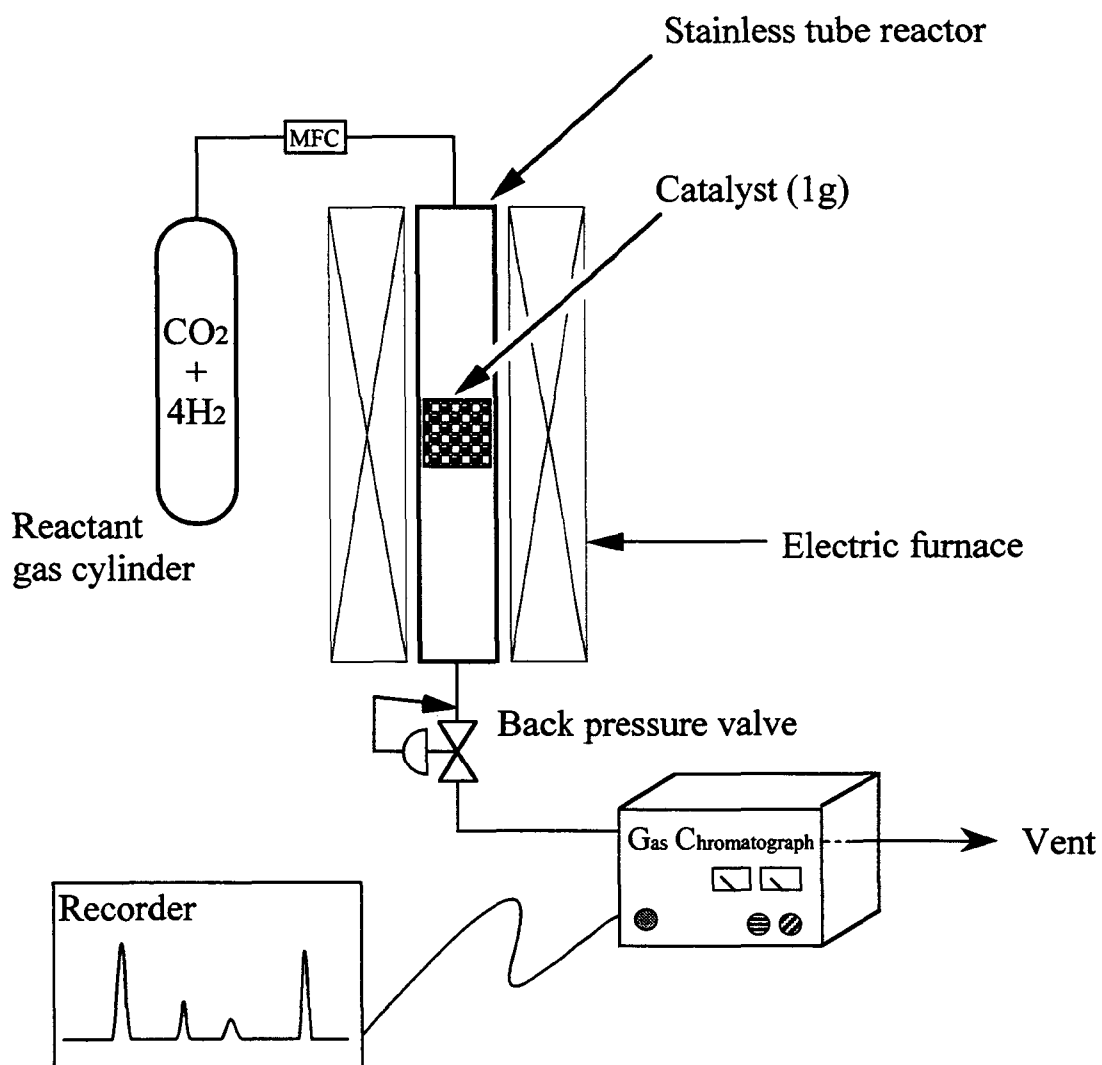
Figure 1.1. A reaction apparatus for the hydrogenation of CO_2.

atmosphere. The ingots were pulverized by hydrogen absorption into powder, then sieved into 0.07-0.11 mm particles.

In a typical experiment 1.0 g intermetallic compound was packed in the stainless tube reactor as shown in Figure 1.1. Pretreatment was carried out with a stream of diluted hydrogen (1% H_2 in N_2) at the rate of 100 ml min^{-1} under atmospheric pressure at 250 °C for 12 h, then the reaction gas (H_2/CO_2=4) was introduced under 5 MPa at the rate of 50 ml min^{-1}. The effluent gas was analyzed with an on-line gas chromatograph using a packed column of MS-13X (4 m). The hydrogen chemisorption was carried out with a Quantasorb Jr.

1.3. Results and discussion

The hydrogenation of carbon dioxide took place under 5 MPa at a reaction temperature as low as 250 °C over $LaNi_4X$. The exclusive product was methane (eq. 1.1), and a small amount of ethane was obtained (Table 1.1). No carbon monoxide was detected. The conversion of carbon dioxide was 93%

Table 1.1. Catalytic activity of $LaNi_4X$.

X	CO_2 Conv.(%)	Selectivity(%) CH₄	Selectivity(%) C₂H₆	H_2 chemisorption (μmol g-cat^{-1})	TOF ($\times 10^3$ sec^{-1})
Ni	93	98	2	44	79
Cr	93	98	2	48	73
Al	4	100	0	~0	~0
Cu	4	100	0	~0	~0
Ni powder	1	100	0	3	14
Ni₅LaOₓ [a]	8 [b]	90	0	16	19

Conditions: 250 °C, 5 MPa, SV=3,000 ml g-cat^{-1} h^{-1}, 10 h-on-stream.
[a] Coprecipitated catalyst. [b] Selectivity to CO was 10%.

5

$$CO_2 + 4H_2 \longrightarrow CH_4 + 2H_2O \qquad\qquad (1.1)$$
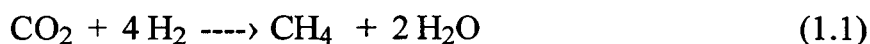
over LaNi$_5$ and the selectivities to methane and ethane in the product were 98% and 2%, respectively. The methanation activities of LaNi$_4$Al and LaNi$_4$Cu were poor at 250 °C. A commercially available nickel powder and Ni$_5$LaO$_x$ catalyst (Ni/La=5 in atomic ratio) prepared by coprecipitation of Ni(NO$_3$)$_2$ and La(NO$_3$)$_3$ showed a slight methanation activity at this temperature.

The hydrogen chemisorption was measured to estimate the number of nickel atoms on the surface of the sample (Table 1.1). The methanation activity corresponded to the amount of the hydrogen adsorbed on the nickel. The turnover frequency (TOF), defined as the number of CO$_2$ molecules converted to methane per active site per unit time, for each catalyst was determined from the hydrogen chemisorption (Table 1.1). It is reported that the value of TOF for the hydrogenation of carbon monoxide over LaNi$_5$ is 2.7×10^{-3} s^{-1} at 205 °C [8]. A comparable TOF value has been obtained even in the reaction with CO$_2$ (see Table 1.1).

The pressure dependence on the hydrogenation of carbon dioxide was carried out over LaNi$_5$ (Table 1.2). The conversion of carbon dioxide over LaNi$_5$ increased with increase in pressure of the reactants. However, even under atmospheric pressure, 56% of carbon dioxide converted to methane and carbon monoxide with the selectivities of 98% and 2%, respectively. A small amount of ethane was obtained as a minor product under high pressures. BET surface area determined by krypton adsorption was less than 1.5 m^2 g^{-1} for all catalysts taken out from the reactor.

To confirm the structure of LaNi$_4$X after the reaction, we recorded the XRD patterns for each catalyst taken out from the reactor after 6 h on the reaction stream. As shown in Figure 1.2, the peaks attributed to metallic nickel (2θ=44.7°, 52.2°) appeared in the patterns for LaNi$_5$ and LaNi$_4$Cr which were

6
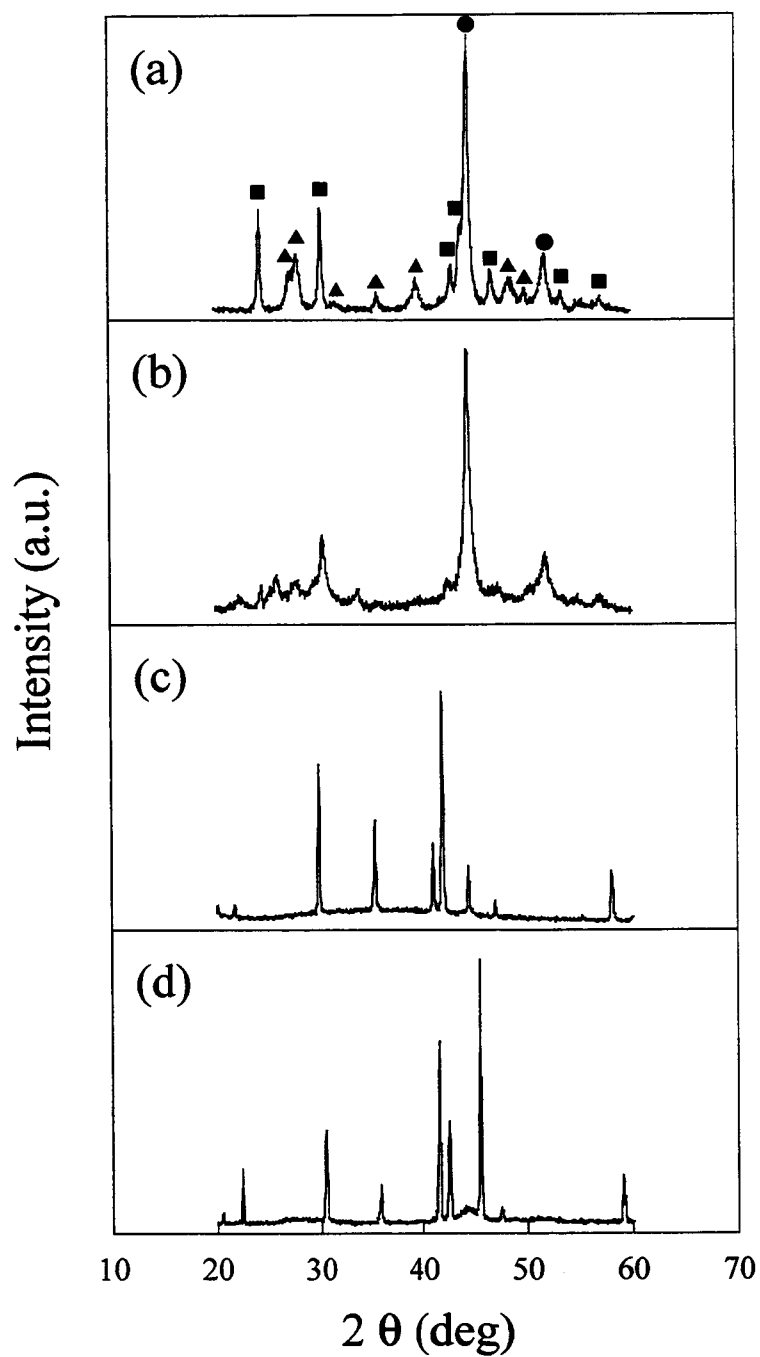
Figure 1.2. XRD patterns of LaNi$_4$X after CO$_2$ methanation.
Target, Cu-Kα; (a)LaNi$_5$, (b)LaNi$_4$Cr, (c)LaNi$_4$Al, (d)LaNi$_4$Cu.
(●) Peaks attributed to Ni; (■) peaks attributed to LaCO$_3$OH;
(▲) peaks attributed to La(OH)$_3$.

Table 1.2. Influence of reaction pressure.

Total pressure (MPa)	CO$_2$ Conversion (%)	Selectivity (%)	
		CH$_4$	C$_2$H$_6$
0.1	56[a]	98	0
1	82	99	1
2	89	99	1
3	92	99	1
4	94	99	1
5	95	99	1

Conditions: LaNi$_5$, 300 °C, SV=3,000 ml g-cat^{-1} h^{-1}, 10 h-on-stream.
[a] Selectivity to CO was 2%.

active catalysts, while these two samples were completely decomposed and no longer had hydrogen storage ability. The peaks for LaCO$_3$OH and for La(OH)$_3$ were also observed. However, no peaks due to metallic nickel were found in the XRD patterns of LaNi$_4$Al and LaNi$_4$Cu. Although these two catalysts are supposed to retain the hydrogen storage ability, the catalytic activities were poor. There is no correlation between the hydrogen storage ability and the catalytic ability. The source of the activity can be mainly attributed to the new sites generated by the decomposition of the intermetallic compounds, and metallic nickel on the surface could be the active site for the reaction. However, nickel powder and Ni$_5$LaO$_x$ obviously containing metallic nickel were less active, suggesting that the activity is not simply due to the metallic nickel. Lanthanum carbonate appeared in the catalyst by the interaction between lanthanum and carbon dioxide during the reaction. Hence, carbon dioxide could be activated on the surface of the lanthanum compound such as lanthanum hydroxide which is basic. Inui and Takeguchi reported that the

existence of lanthanum oxide was effective for the methanation [10]. Yamashita et al. also pointed out the importance of the interaction between nickel and lanthanum in amorphous alloy for the generation of active sites to the carbon monoxide hydrogenation [11]. The contribution of lanthanum to the catalysis will be discussed in chapter 3.

1.4. References

[1]   K. Soga, H. Imamura, S. Ikeda, *Chem. Lett.*, 1387(1976).

[2]   K. Soga, H. Imamura, S. Ikeda, *J. Phys. Chem.*, 81(1977)1762.

[3]   J. Barrault, A. Guilleminot, A. Percheron-Guegan, V. Paul-Boncour and J. C. Achard, *J. Less-Common Met.*, 131(1987)425.

[4]   J. R. Johnson, Z. Gavra, P. Chyou, and J. J. Reilly, *J. Catal.*, 137(1992)102.

[5]   A. Elattar, T. Takeshita, W. E. Wallace and R. S. Craig, *Science*, 196(1977)1093.

[6]   A. F. Andresen and A. J. Maeland, (eds.), *Hydrides for Energy Storage*, Pergamon, Oxford, England, 1978, p.501.

[7]   R. S. Craig, W. E. Wallace, H. Kevin Smith, *Science and Technology of Rare Earth Materials*, Academic Press, Inc., 1980, p.353.

[8]   A. Elattar, W. E. Wallace, and R. S. Craig, *Adv. Chem. Ser.*, 178(1979)7.

[9]   J. Barrault and D. Duprez, *J. Less-Common Met.*, 89(1983)537.

[10]   T. Inui and T. Takeguchi, *Catal. Today*, 10(1991)95.

[11]   H. Yamashita, M. Yoshikawa, T. Funabiki, S. Yoshida, *J. Catal.*, 99(1986)375.

Chapter 2

Hydrocarbon Synthesis from Carbon Dioxide over Fe-Cu Catalysts

2.1. Olefin formation from carbon dioxide over Fe-Cu catalyst

2.1.1. Introduction

The Fischer-Tropsch (F-T) type iron catalyst is often employed for the hydrocarbon synthesis from carbon oxides, and many researchers are still engaged in the development of both the catalyst and the reaction system [1-15]. Alkali metals are effective additives for iron catalysts to increase selectivity to olefin compounds [1-4, 16-21].

It is known that the addition of alkali metals enhances adsorption of carbon oxides on the reduced iron but adsorption of hydrogen is rather weakened [22-24]. This may relate to the increase in the selectivity to olefins, and Arakawa and Bell reported that the hydrogenation of carbon monoxide over iron catalysts results in formation of olefins in presence of potassium on the surface [22].

Although it is believed that iron carbide is an active phase for the F-T synthesis [25-27], formation of the carbide phase must be prevented in presence of carbon dioxide in the feed stock because the reaction between carbon and carbon dioxide to carbon monoxide is expected to take place. In this section, we have investigated the reaction with carbon dioxide over copper-promoted iron (Fe-Cu) catalysts, which is a typical F-T catalyst, to clarify the surface phase of the catalyst.

10

2.1.2. Experimental

Fe-Cu catalysts were prepared by coprecipitation from an aqueous solution containing iron and copper nitrates (the concentration of the metals was 1 M) and an aqueous solution of NaOH (1 M). The precipitates were washed with distilled water, then, dried in air at 120 °C for 6 h. The resulting solids were calcined in air at 350 °C for 3 h, and were ground into powders (100-400 mesh). The bulk composition of the catalysts was determined by ICP emission spectrometry (Table 2.1.1).

Table 2.1.1. Chemical composition of Fe-Cu catalysts.

Sample	Content (wt%)				BET surface area $(m^2\ g^{-1})$ [a]
	Fe	Cu	Na	O	
$FeCu_{0.99}$	33.3	37.6	<0.01	29.1	5
$FeCu_{0.26}$	52.7	15.3	<0.01	32.0	5
$FeCu_{0.11}$	62.8	8.00	0.08	29.1	10
$FeCu_{0.06}$	64.8	4.77	0.06	30.4	8
$FeCu_{0.01}$	69.3	0.49	<0.01	30.2	5
$FeCu_{0.05}Na_{0.07}$	62.6	3.86	1.75	31.8	5
$FeCu_{0.01}Na_{0.01}$	68.7	0.74	0.40	30.2	6

[a] Determined by nitrogen physisorption after reaction.

The catalytic hydrogenation of carbon dioxide was performed with a fixed-bed flow reactor made of stainless steel tube with 9.0 mm I.D as shown in chapter 1. A catalyst (1.0 g) was pretreated with diluted hydrogen (1 vol% H_2 in N_2) at 250 °C under atmospheric pressure for 12 h. After introduction of a reaction gas mixture (25 vol% CO_2 in H_2) at 250 °C, the pressure was raised to 5 MPa (total flow rate, 3.0 $dm^3\ h^{-1}$ in S.T.P.); then, the reaction temperature was

Table 2.1.2. Hydrogenation of carbon dioxide over Fe-Cu catalysts.

Catalyst	CO_2 conv.(%)	Yield(C-mol%)								
		CO	C_1	C_2	C_3	C_4	C_5	C_6	C_7	C_8
CuO	13	10.4	2.6	0	0	0	0	0	0	0
$FeCu_{0.99}$	39	11.6	10.0	4.6	5.2	3.4	2.2	1.5	0.7	0.3
$FeCu_{0.26}$	40	12.4	12.2	4.7	4.5	2.7	1.6	1.2	0.3	0.1
$FeCu_{0.11}$	40	8.3	7.7	3.9	5.6	5.0	3.9	3.3	1.9	0.8
$FeCu_{0.06}$	40	8.1	7.2	3.9	5.6	4.9	3.9	3.4	2.0	1.4
$FeCu_{0.01}$	39	12.1	13.7	4.4	4.0	2.1	1.5	0.7	0.3	0.1
$FeCu_{0.05}Na_{0.07}$	41	7.4	7.8	3.7	5.7	5.6	4.2	3.7	2.0	0.5
$FeCu_{0.01}Na_{0.01}$	40	6.8	7.1	3.9	6.1	6.0	4.3	3.7	2.3	0.4
Fe_2O_3	8 [a]	6.3	1.0	0	0	0	0	0	0	0

Conditions: temperature, 400 °C; pressure, 5 MPa; Space velocity, 3,000 ml g-cat^{-1} h^{-1}; time-on-stream, 2 h.

[a] MeOH was observed with 0.7% yield.

gradually raised to 400 °C. The effluent gas was analyzed with on-line gas chromatographs of which columns were Porapak Q for CO_2 , MS-13X for methane and CO, PLOT (Fused Silica, Al_2O_3/KCl) for hydrocarbons, and PEG-6000(15%)+TCEP(8%) supported on Chromosorb WAW(60/80 mesh) for alcohols. Yields and selectivities were calculated on the basis of carbon numbers in the products.

2.1.3. Results

Carbon dioxide was hydrogenated into carbon monoxide and hydrocarbons at 400 °C over the Fe-Cu catalysts (Table 2.1.2). Methanol was

Table 2.1.3. Olefin content in the hydrocarbon products.

Catalyst	Time-on-stream (h)	Olefin content (%)		
		C_2	C_3	C_4
$FeCu_{0.99}$	2	0	0	0
	24	0	0	0
$FeCu_{0.26}$	2	0	0	0
	27	0	0	0
$FeCu_{0.11}$	2	0.3	0.8	1.3
	24	2.6	24.1	32.4
$FeCu_{0.06}$	2	0	0.5	0.6
	25	1.8	11.3	20.8
$FeCu_{0.01}$	2	0	2.6	9.7
	24	1.6	27.9	37.9
$FeCu_{0.05}Na_{0.07}$	2	1.2	22.0	29.7
	23	34.2	71.7	74.0
	47	51.1	77.0	78.6
$FeCu_{0.01}Na_{0.01}$	2	21.8	62.0	63.7
	27	57.8	72.4	83.2

also produced but the yield was negligibly small. The conversions of carbon dioxide were ca. 40%, regardless of the catalyst composition and the surface area (5-10 m^2 g^{-1}, after reaction; see Table 2.1.1). The yields of methane and carbon monoxide related roughly and were essentially high in the products. When the molar ratio of Cu/Fe in the catalyst was 0.11 or less, olefins were formed in the reaction (Table 2.1.3). The olefin selectivity was always high in C_4 products and decreased with decrease in the carbon number. At the initial stage of the reaction over $FeCu_{0.01-0.11}$ the selectivities to olefins were small, but they increased with increase in time-on-stream. The selectivities were significantly high with $FeCu_{0.05}Na_{0.07}$ and $FeCu_{0.01}Na_{0.01}$ and they also increased with increase in time-on-stream.

XRD patterns were recorded with the catalysts taken out from the reactor after the reaction. There were peaks attributed to Fe_3O_4 (18.3, 30.1, 35.4, 37.1, 43.1, 53.4, and 56.9° in 2θ) in the patterns but no peaks attributed to metallic iron were observed [29]. The crystalline size of Fe_3O_4 was determined as ca. 40 nm for all samples from the width of the peak at 35.4° using the equation of Scherrer [30]. Slight peaks for iron carbide were present in the pattern for $FeCu_{0.01}Na_{0.01}$. The peaks attributed to metallic copper (43.3 and 50.4°) were also found in the patterns but the intensities were weak for the samples whose Cu/Fe molar ratios are 0.01-0.06 [29]. A discernible peak was recorded at 36° attributed to Cu_2O only with $FeCu_{0.99}$ [29]. It is noteworthy that there were peaks at 24.6 and 31.9° attributed to $FeCO_3$ in the pattern for $FeCu_{0.05}Na_{0.07}$ [29].

XPS analyses were performed with the Fe-Cu catalysts after the reaction. Although the XRD analysis shows the presence of Fe_3O_4, the binding energy of Fe($2p_{3/2}$) for the catalysts taken out after the reaction was 710.3-709.9 eV which is significantly smaller than that for Fe_3O_4 at 711 eV [28,31,32]. The binding energy is rather close to that for FeO [28,31,32], appearing that the
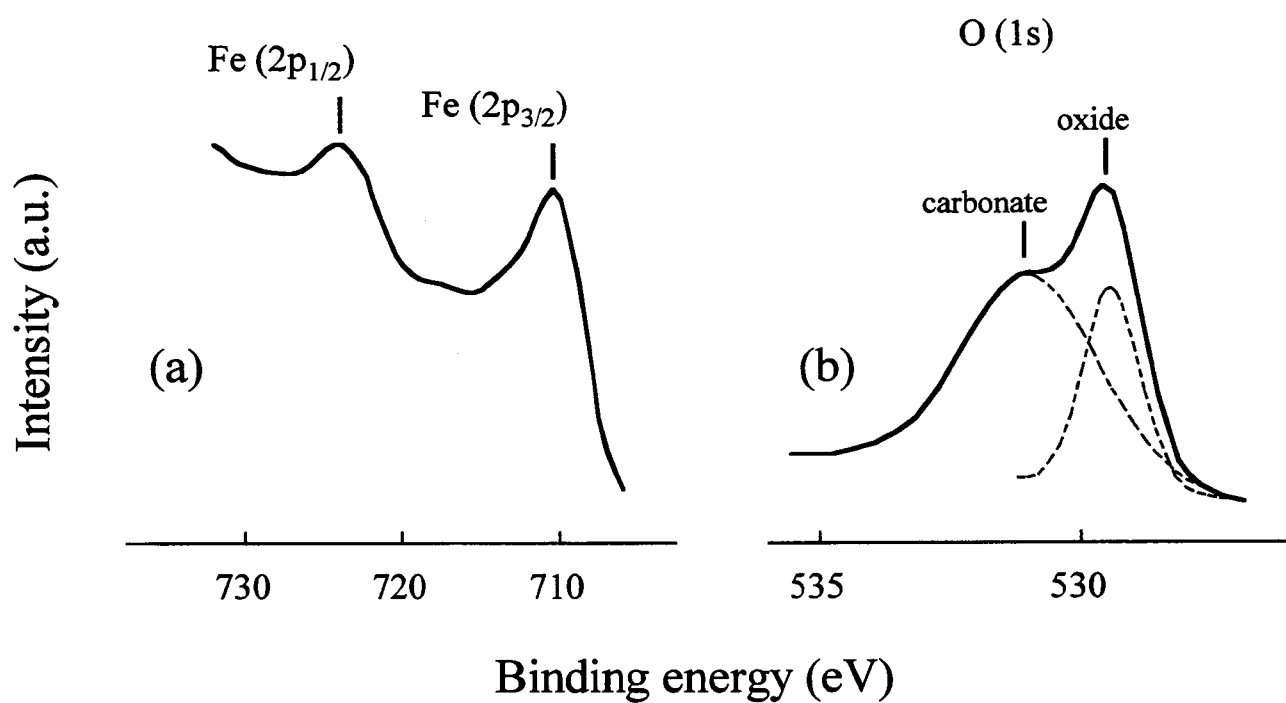
Figure 2.1.1. X-ray photoelectron spectra for $FeCu_{0.01}Na_{0.01}$ after 27 h reaction; (a) $Fe(2p_{1/2})$ and $Fe(2p_{3/2})$, (b) $O(1s)$.

surface of the Fe-Cu catalysts is reduced to FeO [28,31]. No peak or shoulder attributed to iron carbide or metallic iron was recorded in the spectra (Figure 2.1.1a) while the binding energy of $Fe(2p_{3/2})$ reported is ca. 707 eV [20]. The binding energy of $Cu(2p_{3/2})$ for the catalysts after reaction was 932.5-932.6 eV almost identical with that for metallic copper (932.7 eV) and far from that for $CuFe_2O_4$ (933.8 eV) [32].

The peak for $O(1s)$ can be divided into two peaks at 529.5-530.2 eV and 531.0-532.3 eV; the former can be attributed to iron oxide and the latter carbonate species (see Figure 2.1.1b) [28]. The peak at 287.6-288.9 eV attributed to carbonate species can be also separated from that for carbon contaminant [28]. The surface composition was calculated from the XPS peak areas using atomic sensitivity factors, 3.00 for $Fe(2p_{3/2})$, 0.66 for $O(1s)$, 6.30 for $Cu(2p_{3/2})$, 0.25 for $C(1s)$, and 2.30 for $Na(1s)$ (Table 2.1.4). The surface compositions of Cu in $FeCu_{0.01}$ and $FeCu_{0.01}Na_{0.01}$ were 10 and 7 mol%, respectively, significantly larger than the chemical contents. A single peak of $Na(1s)$ was recorded and the binding energy was 1071.5-1072.1 eV. The surface concentrations of sodium were 3-5 mol% for $FeCu_{0.01-0.99}$ and 13 mol% for $FeCu_{0.05}Na_{0.07}$ and $FeCu_{0.01}Na_{0.01}$, showing that sodium is dominantly present on the surface. However, the values for $FeCu_{0.01-0.99}$ were considerably smaller than the concentration of carbonate species, the carbonate species are rather $FeCO_3$ than Na_2CO_3.

2.1.4. Discussion

When carbon dioxide is used as a carbon source in the hydrocarbon synthesis, it is known that carbon monoxide is formed in the reverse water gas shift reaction and further hydrogenated to hydrocarbons [33]. Hence the reaction mechanism with carbon dioxide should be similar to that of the Fischer-Tropsch reaction, however, the distribution of produced hydrocarbons over the

Fe-Cu catalyst whose Cu/Fe molar ratio is less than 0.11 ($FeCu_{<0.11}$) did not follow the Schulz-Flory distribution function. As described above the olefin content in the product was high over $FeCu_{<0.11}$, and this might lead to the deviation from the Schulz-Flory equation. The detail reaction mechanism is under investigation.

Since the equilibrium conversion of carbon dioxide to carbon monoxide under the reaction conditions (400 °C, 5 MPa) is 46% , the equilibrium could govern the total conversion because the conversions of carbon dioxide in Table 2.1.2 are close to the equilibrium value regardless of the catalysts. Despite the similar conversion, the total yields of hydrocarbons do not always the same (see Table 2.1.2). The catalytic activity does not depend on the content or surface concentration of copper in $FeCu_{0.01-0.99}$ but does on the concentration of sodium, that is, $FeCu_{0.05}Na_{0.07}$ and $FeCu_{0.01}Na_{0.01}$ produced 32-34% of total hydrocarbons. Kölbel et al. showed that copper is an important promoter for iron catalysts but the content is not affect to the activity [19], and Wachs et al. also reported that the product distribution do not change when copper is incorporated into an iron catalyst [20]. These are consistent with our results. It is known that significant promotional effect appears with simultaneous presence of copper and alkali metal in the hydrogenation of carbon monoxide over iron catalysts [33], and it is consistent with our results. In general, presence of alkali metals on iron catalysts results in formation of olefin compounds in the Fischer-Tropsch synthesis and it is pointed out that basic sites on the catalysts play an important role for production of olefins [34]. Actually, the formation of carbonate species found in the XPS analyses of the used catalysts suggests the presence of basic sites on the surface. The strength of the basicity can relate to the binding energy of O(1s) for the carbonate species because the electron density of oxygen is expected to be high on basic sites. Figure 2.1.2 shows the relation between the olefin

Table 2.1.4. Surface composition (mol%) of the Fe-Cu catalysts determined by XPS.

Catalyst	Na	Cu	Fe	O		C
				oxide	carbonate	carbonate
$FeCu_{0.99}$	3	31	11	18	28	9
$FeCu_{0.26}$	2	30	17	24	21	6
$FeCu_{0.11}$	3	20	17	16	35	9
$FeCu_{0.06}$	5	4	25	25	31	10
$FeCu_{0.01}$	3	10	28	20	31	8
$FeCu_{0.05}Na_{0.07}$	13	13	14	13	34	13
$FeCu_{0.01}Na_{0.01}$	13	7	17	14	36	13
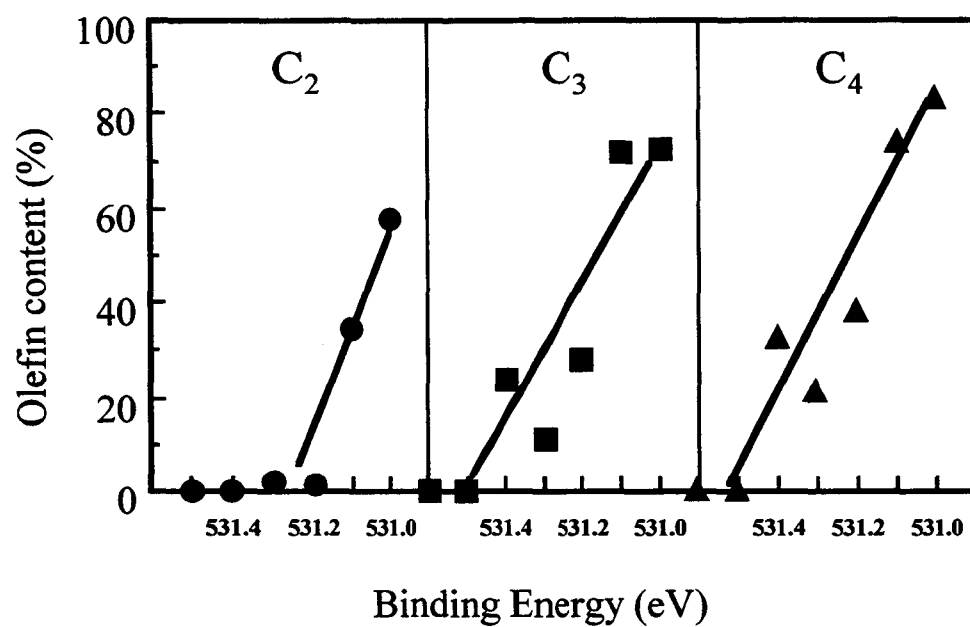
Figure 2.1.2. Relationship between the binding energy of O(1s) for carbonate species and olefin content.

contents in the C_2-C_4 products and the binding energy of O(1s) for carbonate species, and the olefin contents at the end of the reaction evidently increase with a decrease in the binding energy, that is, an increase in basicity.

Since the binding energy of O(1s) for the carbonate is low in the catalysts with high surface concentration of sodium ($FeCu_{0.05}Na_{0.07}$ and $FeCu_{0.01}Na_{0.01}$), sodium ions on the catalysts are the source of the basicity. The binding energies of Fe(2p$_{3/2}$) for these catalysts were low, showing interaction between iron and sodium ions. However, $FeCu_{0.99}$ and $FeCu_{0.26}$ whose surface concentrations of sodium are not negligible did not produce olefin compounds. Although the binding energies of Fe(2p$_{3/2}$) evidence that FeO is the dominant species on these catalysts, the atomic ratios of O(oxide)/Fe are significantly larger than one while the ratios for other catalysts producing olefins are close to one (see Table 2.1.4). This suggests that the dominant surface phases of FeO in these two catalysts are different from the others. Sodium ions are considered to coordinate to iron via oxygen atoms, hence, high density of oxygen may increase the coordination number of sodium and decrease basicity. Formation of $FeCO_3$ is evidenced from the XRD pattern of $FeCu_{0.01}Na_{0.01}$ taken out after the reaction of 47 h. The absence of the peak attributed to $FeCO_3$ in other patterns for the catalysts endured for 27 h or less suggests gradual reduction of Fe_3O_4 on the surface to FeO or $FeCO_3$. Hence, it may be supposed that the gradual phase transfer results in increase in the olefin selectivity with time-on-stream. The surface densities of copper for $FeCu_{0.99}$ and $FeCu_{0.26}$ are high and it could be possible that hydrogenation activity of copper suppresses olefin formation. Formation of olefin has been proposed to be caused by stronger adsorption of carbon monoxide on basic sites where carbon monoxide is not perfectly reduced to alkanes [35]. However, in the hydrogenation of carbon dioxide the ratio of H_2/CO is very high, and this implies the presence of different mechanisms such as

stabilization of olefinic species on basic sites, while further investigation is necessary to clarify it.

2.1.5. References

[1] M. Röper, "Catalysis in C_1 Chemistry", ed. W. Keim, D. Reidel Publishing Co., Dordrecht (1983).

[2] H. Pichler, "Advances in Catalysis", vol. 4, eds. Frankenburg, Komarewsky, and Rideal, Academic Press, (1952)271.

[3] M. E. Dry, "Catalysis Science and Technology", vol. 1, eds. J. R. Anderson and M. Boudart, Springer-Verlag, New York, (1982)159.

[4] Min-Dar Lee, Jyh-Fu Lee and Chau-Shang Chang, *Bull. Chem. Soc. Jpn.*, 62(1989)2756.

[5] J. Barrault, C. Forquy, J. C. Menezo and R. Maurel, *React. Kinet. Catal. Lett.*,17(1981)373.

[6] M. Fujiwara and Y. Souma, *J. Chem. Soc., Chem. Commun.*, (1992)767.

[7] D. J. Dwyer and G. A. Somorjai, *J. Catal.*,52(1978)291.

[8] M. Pijolat, V. Perrichon, M. Primet and P. Bussiére, *J. Mol. Catal.*, 17(1982)367.

[9] A. Kiennemann, R. Kieffer, E. Chornet, *React. Kinet. Catal. Lett.*, 16(1981)371.

[10] Raymond C. Everson and Harko Mulder, *J. Catal.*, 143(1993)166

[11] Jean-Claude Carlu and Claude Caze, *React. Polym.*, 12(1990)187.

[12] G. D. Weatherbee and C. H. Bartholomew, *J. Catal.*,87(1984)352

[13] T. Inui, T. Takeguchi, A. Kohama, and K. Kitagawa, "New Frontiers in Catalysis", vol. B, ed. L. Guczi, (1993)1453.

[14] R. J. Madon and W. F. Taylor, *J. Catal.*, 69(1981)32.

[15] T. Inui and T. Takeguchi, *Catal. Today*, 10(1991)95.

[16] S. Soled, E. Iglesia, and R. A. Fiato, *Catal. Lett.*,7(1990)271.

[17] N. O. Egiebor and W. C. Cooper, *Appl. Catal.*, 17(1985)47.

[18] D. J. Dwyer and G. A. Somorjai, *J. Catal.*,56(1979)249.

[19] H. Kölbel, P. Ackermann, E. Ruschenburg, R. Langheim, F. Engelhardt, *Chem. Ing. Tech.*,23(1951)153.

[20] I. E. Wachs, D. J. Duyer, E. Iglesia, *Appl. Catal.*, 12(1984)201.

[21] Dragomir B. Bukur, Doble Mukesh, and Snehal A. Patel, *Ind. Eng. Chem. Res.*,29(1990)194.

[22] Hironori Arakawa and Alexis T. Bell, *Ind. Eng. Chem. Process Des. Dev.*, 22(1983)97.

[23] J. Benziger and R. J. Madix, *Surf. Sci.*,94(1980)119.

[24] M. E. Dry, T. Shingles, L. J. Boshoff, and G. J. Oosthuizen, *J. Catal.*, 15(1969)190.

[25] P. Biloen, J. N. Helle, and W. M. H. Sachtler, *J. Catal.*,58(1979)95

[26] J. W. Niemantsverdriet, A. M. van der Kraan, W. L. van Dijk, and H. S. van der Baan, *J. Phys. Chem.*,84(1980)3363.

[27] Ronald A. Dictor and Alexis T. Bell, *J. Catal.*,97(1986)121.

[28] C. D. Wagner, W. M. Riggs, L. E. Davis, J. F. Moulder, and G. E. Muilenberg (Editor), "Handbook of x-ray photoelectron spectroscopy", Perkin-ElmerCorp.,1978.

[29] JCPDS powder diffraction file: Fe_3O_4, 19-629; Cu, 4-836; Cu_2O,35-1091; $FeCO_3$,29-696.

[30] H. P. Klug and L. E. Alexander, "X-ray Diffraction Procedures", John Wiley and Sons Inc., New York, 1954.

[31] J. P. Baltrus, J. R. Diehl, M. A. McDonald and M. F. Zarochak, *Appl. Catal.*,48(1989)199.

[32] C. D. Wagner, "Practical Surface Analysis vol. 1", D. Briggs and M. P. Seah Eds.,p.595.

[33]   M. Pijolat, V. Perrichon, M. Primet and P. Bussière, *J. Mol. Catal.,* 17(1982)367.

[34]   M. E. Dry and G. J. Oosthuizen, *J. Catal.,* 11(1968)18.

[35]   M. E. Dry, T. Shingles, L. J. Boshoff, and G. J. Oosthuizen, *J. Catal.,* 15(1969)190.

2.2. Effect of water on the hydrogenation of carbon oxides

2.2.1. Introduction

The transformation of CO_2 into useful chemicals such as hydrocarbons is an option for reduction of CO_2. Since Fe-based catalysts have been widely used in the water gas shift (WGS) reaction [1] as well as Fischer-Tropsch (F-T) reaction [2-9], Fe is a candidate as a catalyst for the hydrogenation of CO_2. However, the hydrogenation of CO_2 over Fe catalyst is difficult for practical use at present because of its much less reactivity than CO [10-13]. In addition H_2O produced by reverse water gas shift (RWGS) reaction may lead to deactivation of the Fe catalyst. Hence, the consideration about the difference in catalyst surface affected by H_2O in the reaction with CO and CO_2 should be necessary to develop new catalyst for CO_2 hydrogenation.

It is known that F-T synthesis over Fe catalyst produces both hydrocarbons and oxygenates. The active phase for hydrocarbon formation is believed to be FeC_x. Miller and Moskovits showed different pathway for oxygenate formation and this implies presence of other active phases [14]. However, identification of the active phases is not easy because the surface iron is not stable during the reaction. That is, formation of FeC_x species accompanies accumulation of carbon on the surface and in case of Fe_2O_3, which is often used as a catalyst precursor, reduction of the oxide to Fe_3O_4 and to metallic Fe also proceed [6].

In this section, we have carried out the hydrogenation of CO and CO_2 over Fe catalyst and compared the catalytic activity and the difference in the surface phase. We have also carried out the addition of steam into the reactant gas mixture to examine the effect of H_2O on the catalytic activity as well as to clarify the change in the surface phase of the catalyst.

2.2.2. Experimental

Iron catalyst was prepared by calcination of iron hydroxide in air at 500 °C for 3 h. The resulting solid was crashed into < 60 mesh granules by using mortar. The hydrogenation of CO_x was carried out with a fixed-bed flow reactor made of stainless steel tube with 10-mm i.d. A catalyst was pretreated with diluted hydrogen (10 vol% H_2 in N_2) stream (50 sccm) under atmospheric pressure at 500 °C for 1 h. After enough cooling of the reactor a reactant gas mixture (33 vol% CO in H_2 or 25 vol% CO_2 in H_2) was introduced and the pressure was raised to 1 MPa and temperature was set at 250 °C. The effluent gas was analyzed with on-line gas chromatographs of which columns were Porapak Q for CO_2 , MS-13X for methane and CO, PLOT (Fused Silica, Al_2O_3/KCl) for hydrocarbons, and PEG-6000(15%)+TCEP(8%) supported on Chromosorb WAW(60/80 mesh) for alcohols. Yields and selectivities were calculated on the basis of carbon numbers in the products.

The BET surface areas of the catalysts were determined from the isotherms of nitrogen physisorption. X-ray diffraction (XRD) patterns were recorded with a Rigaku ROTAFLEX diffractometer (Cu-Kα, 40 kV, 150 mA). Surface analyses by X-ray photoelectron spectroscopy (XPS) were performed with a Shimadzu ESCA-750. The spectra were recorded after argon-ion etching for 1 min (2 kV, 25 mA). The binding energy was corrected with the energy of C(1s) (284.6 eV) for carbon contaminant [15].

2.2.3. Results and discussion

Catalytic Performance of Fe Catalyst

The catalytic hydrogenation of CO_x over Fe catalyst reduced at 500 °C is summarized in Table 2.2.1. Since the purpose of this study is not to develop a highly active catalyst but to elucidate the factor that controls the catalytic performance in the reaction with CO_x, the reaction conditions described in

25

Table 2.2.1. Hydrogenation of CO_x over Iron Catalyst (Rate of Formation).

Reactant (composition)	CO_x	Hydrocarbons		Alcohols			Selectivity to alcohols [a]
		C_{1-4}	C_{5+}	MeOH	EtOH	PrOH	
H_2/CO (67/33)	20.3	69.3	52.8	22.4	11.6	4.5	24
H_2/CO_2 (75/25)	3.3	7.5	1.0	1.6	0.3	0	12
$H_2/CO/H_2O$ (42/21/37)	20.1	1.1	0.5	1.9	0.2	0	56
$H_2/CO_2/H_2O$ (48/16/36)	0	<0.1	0	0.1	0	0	95 [b]

Conditions: 250 °C, 1 MPa, stable activity.

(unit: μmol g-cat^{-1} h^{-1})

[a] (yields of C_{1-3} alcohols)/(total yield - yield of CO_x)$\times$100

[b] The CO_2 conversion was 0.1%.

Table 2.2.1 were not optimized to get good yield. In the reaction with CO, the major products were C_1-C_9 hydrocarbons, C_1-C_3 alcohols, and CO_2. The product distribution of hydrocarbons was almost obeyed by the Schulz-Flory's law (Figure 2.2.1a). From the plots of the carbon number n vs. $\ln(W_n/n)$, the probability of chain growth, α, was estimated as 0.64. When CO_2 is used as a reactant, C_1-C_5 hydrocarbons, C_1 and C_2 alcohols, and CO were obtained. The distribution of hydrocarbons produced was also followed by the Schulz-Flory's law (Figure 2.2.1b), showing that the hydrogenation of CO_2 proceeds along with the F-T type reaction scheme followed by RWGS reaction. A smaller value of a for CO_2 hydrogenation (0.44) than that obtained in CO reaction reflects the higher selectivity to light hydrocarbons (see Table 2.2.1).

It is noteworthy that the formation rate of CO_2 was almost the same before and after addition of H_2O. The rates of hydrocarbon and alcohol formation were suppressed by addition of H_2O, then totally, the selectivity to alcohols increased (see Table 2.2.1). This means that the site for hydrocarbon formation was deactivated. It is conceivable that H_2O oxidizes the surface iron and this may prevent formation of carbide species. The catalyst seems to have the activity for MeOH formation even after addition of H_2O, while the rates for C_{2+} alcohol production almost diminished (see Table 2.2.1), suggesting that the site for C_{2+} alcohol formation is relevant to that for hydrocarbon formation.

On the other hand, the catalytic activity almost disappeared when H_2O was added to CO_2 hydrogenation. Only trace amount of methane and methanol was observed. The apparent selectivity to alcohols was high due to low conversion of CO_2.

Bulk and surface composition of Fe catalyst

When the reaction finished, the reactant gas was switched to helium gas and the reactor was cooled down to room temperature. The sample was taken
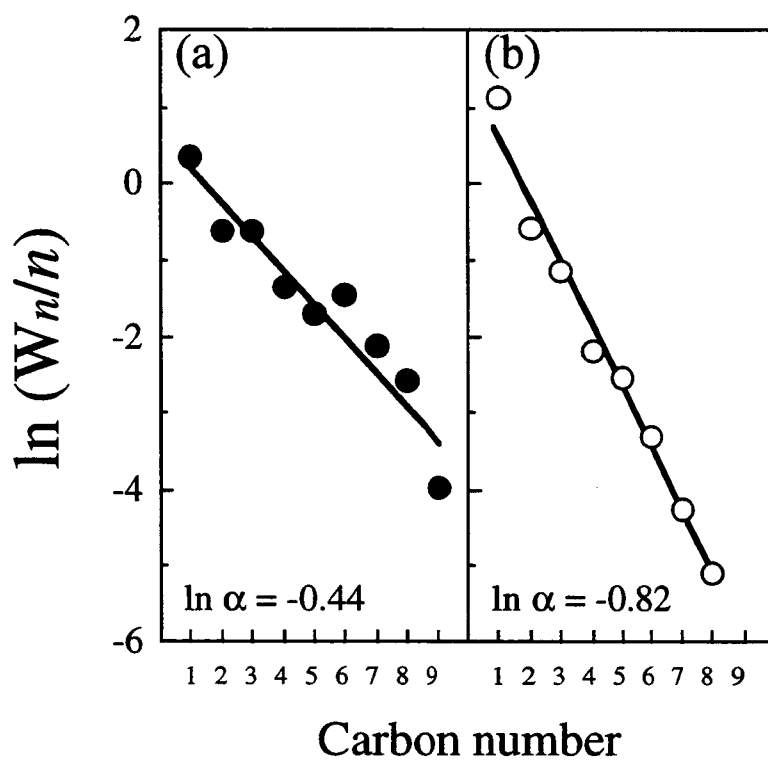
Figure 2.2.1. Schulz-Flory plots for the hydrogenation over iron catalyst reduced at 500 °C. (a), reaction with CO; (b), reaction with CO_2.

Table 2.2.2. Surface Analysis by XPS for Fe Catalysts.

Reactant	Surface composition (mol%)					$[Fe]/[O]^a$
	Fe^0	Fe^{2+}	Fe^{3+}	O_{Fe-OH}	O_{Fe-O}	
---- [b]	13	32	10	16	29	1.2
H_2/CO	19	40	3	17	21	1.6
H_2/CO_2	2	28	14	23	33	0.8
$H_2/CO/H_2O$	0	18	18	40	24	0.6
$H_2/CO_2/H_2O$	0	16	18	42	24	0.5

Conditions: Mg-Kα, 8 kV, 30 mA. Ar$^+$ etching (2 kV, 25 mA) for 60 s was performed before measurement.

[a] [Fe], total amount of Fe species; [O], total amount of O species.

[b] after reduction with H_2/N_2.

out from the reactor and transferred into XRD or XPS instruments in air. It was confirmed that the exposure of samples composed of Fe to air is not a serious drawback for the reliability of the characterization of the catalyst [6, 16].

X-ray diffraction (XRD) analyses showed a clear peak attributed to α-Fe at 44.6° in 2θ for the sample taken out from the reactor just after the reduction at 500 °C (Figure 2.2.2a). The sample taken out from the reactor after the reaction with CO retained the structure and peaks attributed to χ-$Fe_{2.2}C$ were also recorded (Figure 2.2.2b). The sample after the reaction with CO_2 also kept α-Fe structure but no peaks attributed to carbide species were observed (Figure 2.2.2c). This implies that the presence of CO_2 in the reactant can prevent the formation of carbide species which is considered as an intermediate of F-T reaction.

Although no significant change in the structure of the catalyst except formation of carbide species during the hydrogenation of CO was observed by the XRD analyses, change in the oxidation state of the surface iron was detected by recording XPS of the catalysts. In the range of $Fe(2p_{3/2})$ a major peak attributed to Fe^0 was recorded at 706.7 eV in the XPS for the catalyst just after the reduction at 500 °C [15]. The spectrum can be deconvoluted to three Gaussian peaks and minor peaks were at 709.3 and 712.5 eV after the reaction with CO (Figure 2.2.3a). The former can be attributed to Fe^{2+} and the latter to Fe^{3+} [15]. No peak or shoulder attributed to iron carbide was observed. The profiles for O(1s) were also separated into two Gaussian peaks at 529.5 eV and 531.1 eV, the former can be attributed to the oxygen connecting to iron and the latter to the oxygen in hydroxide (O_{Fe-OH}) (Figure 2.2.3b) [15].

The surface composition was calculated by using the atomic sensitivity factors for each element [15] and tabulated in Table 2.2.2. The value of [Fe]/[O] ratio just after the pretreatment was 1.2 and those after the reaction with CO and CO_2 were 1.6 and 0.8, respectively. The amount of metallic iron increased and
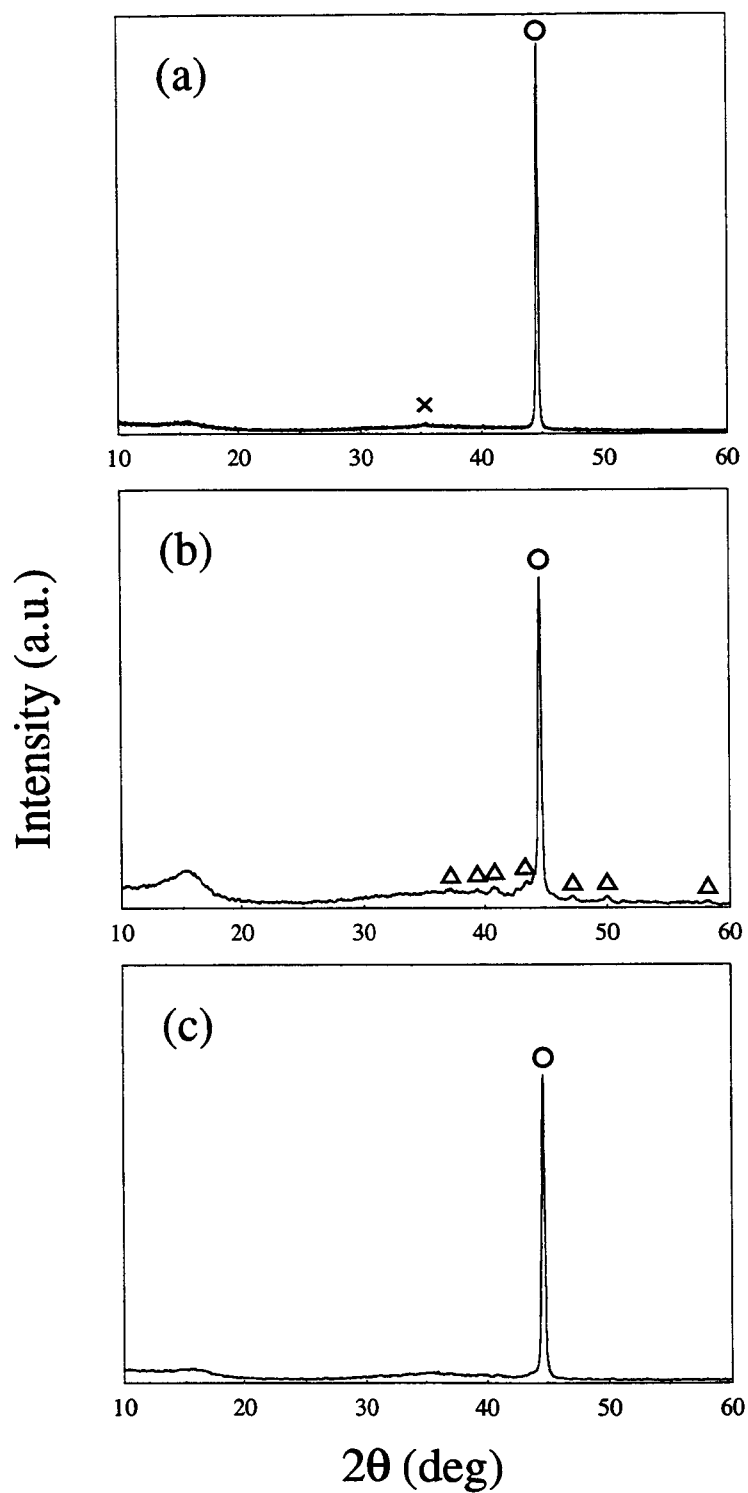
Figure 2.2.2. XRD patterns for iron catalysts: (O)Fe; (X)Fe$_3$O$_4$; (Δ)Fe$_{2.2}$C: (a) after reduction at 500 °C; (b) followed by reaction with CO; (c) followed by reaction with CO$_2$.
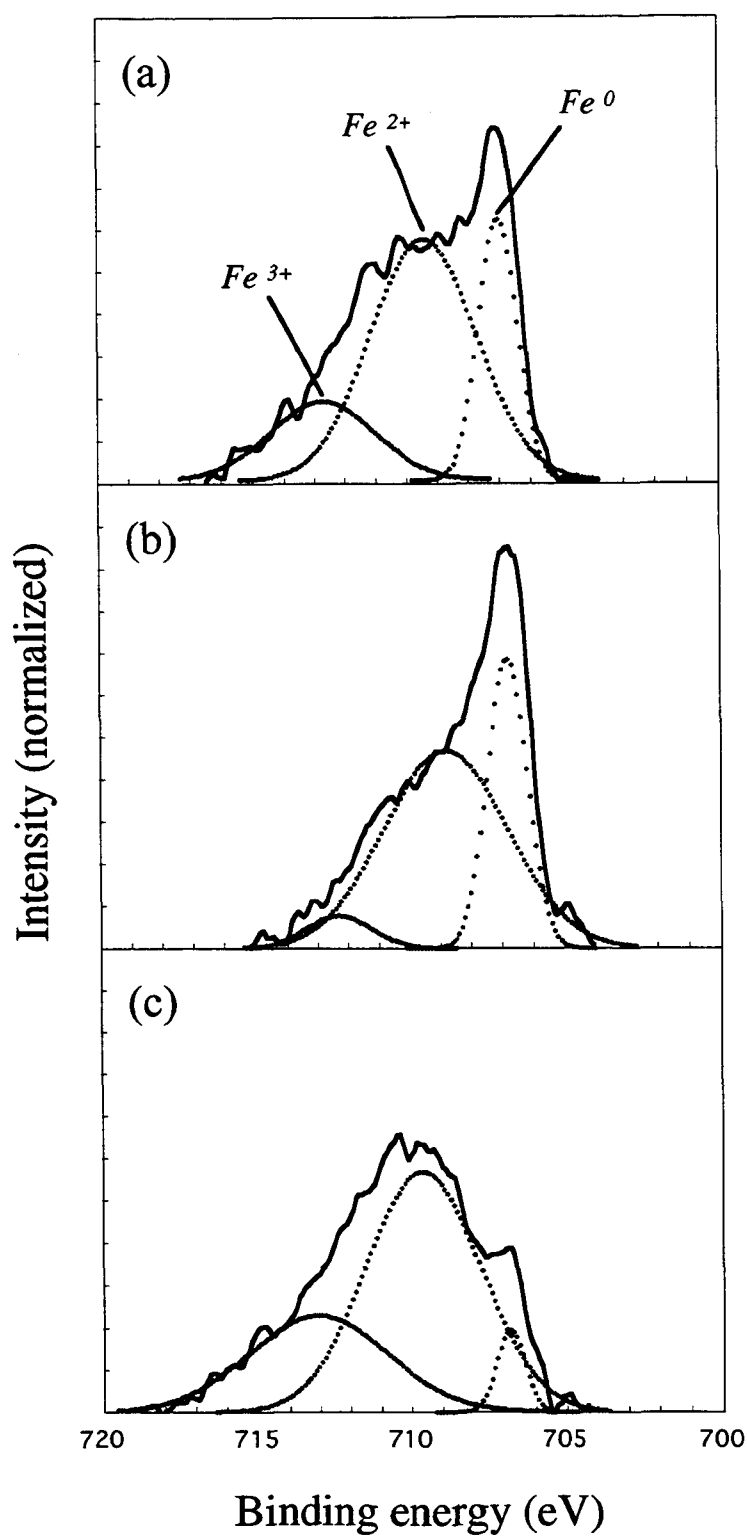
Figure 2.2.3. XPS spectra of $Fe(2p_{3/2})$ for iron catalysts:
(a) after reduction at 500 °C; (b) followed by reaction with
CO; (c) followed by reaction with CO_2.

χ-Fe$_{2.2}$C phase was detected by XRD for the sample after the reaction with CO, showing that the iron carbide is an active species for hydrocarbon formation. Although no metallic iron phase was observed in the sample after addition of steam, the selectivity to alcohol increased. This implies the presence of other active phases to produce alcohols. On the other hand, the surface iron was oxidized after the reaction with CO_2 and this may prevent formation of carbide species, resulting in low hydrocarbon formation.

In the reaction with $H_2/CO/H_2O$, the suppression of the rate of MeOH formation was not so significant while those of C_{2+} alcohol formation were drastically suppressed (see Table 2.2.1). This means that the active site for MeOH formation is different from those for C_{2+} alcohol. Furthermore, the amount of O_{Fe-OH} species increased by addition of steam (see Table 2.2.2), suggesting that the O_{Fe-OH} species plays an important roll for formation of MeOH, however, further investigation is necessary to clarify the details.

2.2.4. References

[1]   David S. Newsome, *Catal. Rev. Sci. Eng.*, 21(2)(1980)275.

[2]   S. Soled, E. Iglesia, R. A. Fiato, *Catal. Lett.*, 7(1990)271.

[3]   D. B. Bukur, D. Mukesh, S. A. Patel, *Ind. Eng. Chem. Res.*, 29(1990)194.

[4]   R. A. Dictor, A. T. Bell, *J. Catal.*, 97(1986)121.

[5]   M. E. Dry, in: *Catalysis Science and Technology*, J. R. Anderson and M. Boudart (Eds.), vol. 1, Springer, New York, 159(1982).

[6]   J. P. Reymond, P. Mériaudeau, S. J. Teichner, *J. Catal.*, 75(1982)39.

[7]   F. Blanchard, J. P. Reymond, B. Pommier, S. J. Teichner, *J. Mol. Catal.*, 17(1982)171.

[8]   R. J. Madon, W. F. Taylor, *J. Catal.*, 16(1981)32.

[9]   G. B. Raupp. W. N. Delgass, *J. Catal.*, 58(1979)361.

[10]   D. J. Dwyer, G. A. Somorjai, *J. Catal.*, 52(1978)291.

[11] J.-F. Lee, W.-S. Chern, M.-D. Lee, T.-Y. Dong, *Can. J. Chem. Eng.*, 70(1992)511.

[12] M.-D. Lee, J.-F. Lee, C.-S. Chang, *Bull. Chem. Soc. Jpn.*,62(1989)2756.

[13] M. Pijolat, V. Perrichon, M. Primet, P. Bussiére, *J. Mol. Catal.*, 17(1982)367.

[14] D. Miller, M. Moskovits, *J. Am. Chem. Soc.*,111(1989)9250.

[15] C. D. Wagner, W. M. Riggs, L. E. Davis, J. F. Moulder, in: *Handbook of X-ray photoelectron spectroscopy*, G. E. Muilenberg (ed), Perkin-Elmer Corp., Minnesota, 1978.

[16] J. A. Amelse, J. B. Butt, L. H. Schwartz, *J. Phys. Chem.*,84(1980)3363.

Chapter 3

Characterization of the Catalyst for
Hydrogenation of Carbon Dioxide

3.1. Phase transformation of LaNi₅ during the reaction with CO_2/H_2

3.1.1. Introduction

Many of hydrogen storage alloys are intermetallic compounds composed of rare-earth metals and transition metals [1]. Their catalytic properties especially for hydrogenation have been extensively investigated because they can store hydrogen as metal hydride which is often active to the hydrogenation of olefins at temperatures lower than 40 °C [2-6]. The alloys can also be applied for the hydrogenation of carbon oxides above 100 °C [7-13]. The catalytic activities of the nickel-based alloys are generally high while under the reaction conditions the structure of the intermetallic compound is changed and the growth of the transition metal particles can be observed.

The catalytic activity of nickel to the hydrogenation of carbon dioxide is known very well [14, 15]. Addition of rare-earth elements to nickel catalysts often results in the enhancement of the activity to the hydrogenation of carbon oxides [12, 16-18]. In the case of lanthanum cobalt intermetallic catalysts, it was shown that the strong interaction between cobalt and the rare-earth causes formation of new active sites [19]. This suggests that interaction between nickel and rare earth elements is important and hydrogen storage alloys are rather good precursors. However, it is not obvious how the rare-earth elements affect the catalytic activity and the further understanding is necessary for the development of the hydrogenation catalysts prepared from hydrogen storage alloys.

35

In this section we will show that the interaction between nickel and lanthanum affects the activity of the catalyst whose precursor is an intermetallic compound of $LaNi_5$ for the hydrogenation of carbon dioxide.

3.1.2. Experimental

An intermetallic compound, $LaNi_5$, was prepared by arc-melting of the metal constituents in a copper crucible under 66.7 kPa of an argon stream. The ingot was pulverized into powder by hydrogen absorption, then the particles of 145-200 mesh were sieved for catalytic tests. A mixed oxide of Ni and La (denoted as Ni_5LaO_x) was prepared by coprecipitation from an aqueous solution of the metal nitrates (0.83 M for Ni^{2+}, 0.17 M for La^{3+}) with a sodium carbonate solution (1 M). The precipitate was well washed with distilled water and dried at 120 °C for 6 h. The solid was calcined in air at 350 °C for 3 h, and crushed into 24 - 40 mesh granules. Nickel powder with the particle size of ca. 210 mesh was obtained from Nihon Kagaku Sangyo Co., Ltd.

The hydrogenation of carbon dioxide was carried out with a fixed-bed flow reactor made of stainless steel tube with 10-mm i.d. A catalyst (1.0 g) was usually pretreated with a hydrogen stream diluted with nitrogen (H_2, 1 mol%) under atmospheric pressure at 250 °C for 12 h. After introduction of a reactant mixture of carbon dioxide (20 mol%) and hydrogen (80 mol%) at 250°C, the pressure was raised to 5 MPa (total flow rate, 3.0 dm^3 h^{-1} in S.T.P.). The effluent gas was analyzed with an on-line gas chromatograph whose columns were Porapak Q for carbon dioxide and MS-13X for methane and carbon monoxide. Yields and selectivities were calculated from the molar fraction of carbon in the products.

X-ray diffraction (XRD) patterns were recorded with a Rigaku ROTAFLEX diffractometer (Cu-Kα). The crystallite size of the catalyst was calculated from the peak width of the XRD pattern using the equation of

Scherrer [20]. Surface analyses by X-ray photoelectron spectroscopy (XPS) were performed with a Shimadzu ESCA-750. The spectra were recorded after argon-ion sputtering for 0.5 min (2 kV, 25 mA). The binding energy was corrected with the energy of $C(1s)$ (284.6 eV) for carbon contaminant [21]. The BET surface areas of the samples were measured with a Quantasorb Jr. by the physisorption of krypton at -196 °C.

3.1.3. Results

Catalytic performance of the catalysts

The hydrogenation of carbon dioxide to methane was carried out over $LaNi_5$ at 250-350 °C. The conversion at 250 °C increased gradually with time-on-stream and the conversion of carbon dioxide reached to ca. 94% at 5 h-on-stream and the catalytic activity became stable (Figure 3.1.1). Trace amounts of carbon monoxide and ethane were formed as by-products, but no C_{3+} hydrocarbons were detected. The catalytic activity increased within 2 h when the reaction temperature was 350 °C. After the reaction at 350 °C for 10 h, the reaction temperature was reduced to 250 °C. The catalytic activity was almost the same as that produced in the reaction at 250 °C for 10 h without the hysteresis, that is, the conversion was 92% (Table 3.1.1). The catalyst reduced at 400 °C for 12 h and that without reduction produced almost the same activity as the one reduced at 250 °C.

In the case of Ni_5LaO_x the catalytic activity was increased during the reaction at 250 °C for 10 h, but the conversion reached was only 8% (see Figure 3.1.1). The CO_2 conversion at 350 °C increased with in 0.5 h-on-stream and the activity was as high as that for $LaNi_5$. However, the conversion at 250 °C after the reaction at 350 °C for 10 h was the same as that without the reaction at 350 °C (see Table 3.1.1). No change in the activity was observed over Ni powder catalyst which produced methane with the conversion of 86% at 350 °C. The

37
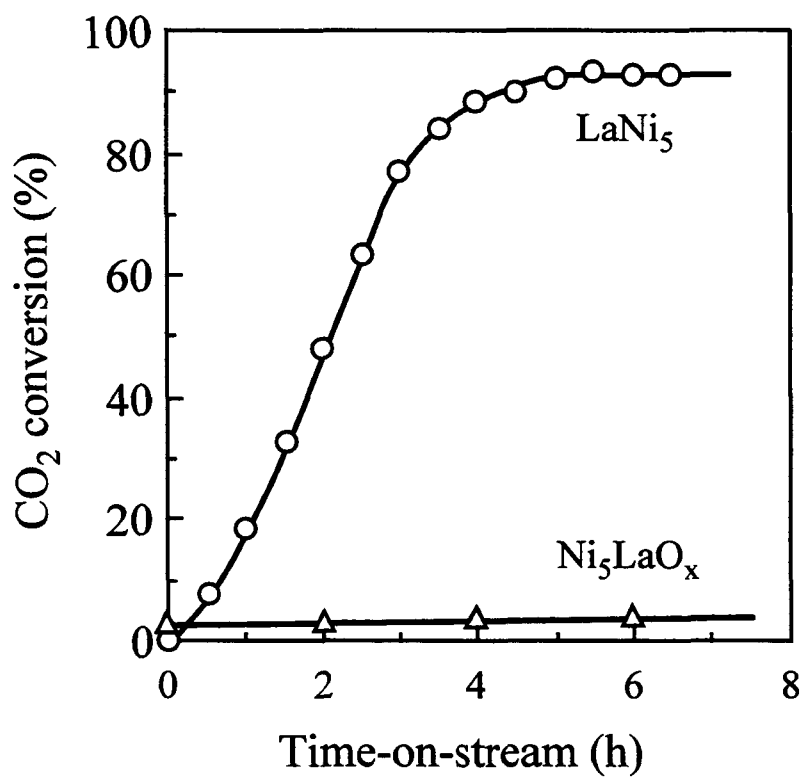
Figure 3.1.1. Hydrogenation of carbon dioxide to methane at 250 °C. (O), LaNi$_5$; ($\triangle$), Ni$_5$LaO$_x$.

conversion at 250 °C was significantly low as 1.1% and that was not increased after the reaction at 350 °C for 10 h.

The BET surface areas were less than 0.1 m^2 g^{-1} for all the samples after the reaction.

Table 3.1.1. Catalytic activities after the reaction at 350 °C for 10 h.

Catalyst	Temp. (°C)	CO_2 conv. (%)	Selectivity (%)		
			CH_4	C_2H_6	CO
LaNi₅	250	93.6	98.1	1.9	0
	300	95.1	98.8	1.2	0
	350	95.1	100	0	0
Ni₅LaOₓ	250	7.9	89.6	0	10.4
	300	54.4	95.3	2.1	2.6
	350	95.4	100	0	0
Ni powder	250	1.1	100	0	0
	300	12.4	100	0	0
	350	85.8	100	0	0

Conditions: 5 MPa, SV=3,000 ml g-cat^{-1} h^{-1}.

XRD analyses

XRD analyses were carried out with different aliquots of LaNi₅ taken out from the reactor just after the pretreatment with H_2 at 250 °C for 12 h and after the reaction for 0.5-6.5 h. A typical XRD pattern of the intermetallic compound was recorded with LaNi₅ just after the pretreatment (Figure 3.1.2a) [22], but the intensity of the peaks was reduced with the time period of the reaction (Figures 3.1.2b-d) and the clear peaks attributed to metallic nickel (2θ = 44.7 and 52.2°) appeared (Figures 3.1.2c-e) [22]. The crystallite sizes of nickel in the samples after the reaction for 4-6.5 h were estimated as 11-18 nm. Lanthanum was
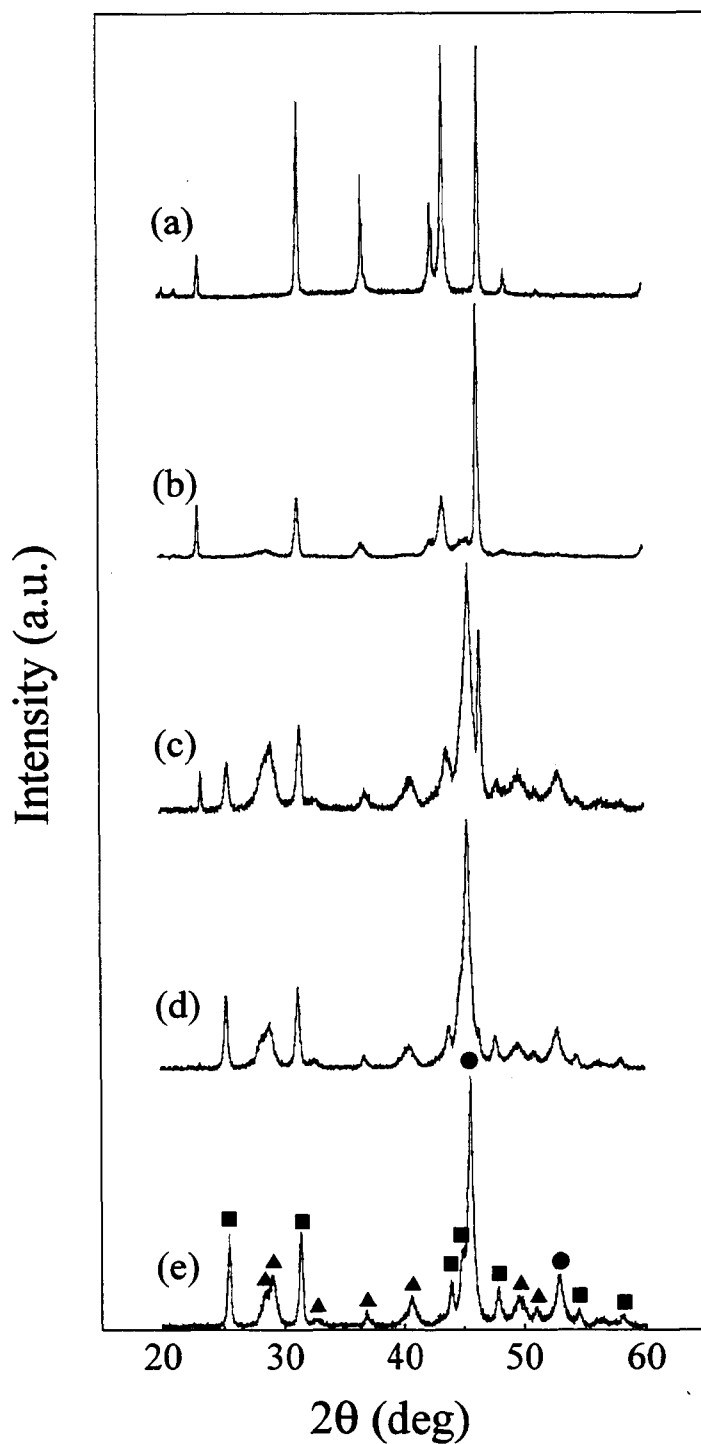
Figure 3.1.2. XRD patterns for LaNi$_5$, (a) just after pretreatment, (b) after reaction at 250 °C for 0.5 h, (c) 2 h, (d) 4 h, (e) 6.5 h. (●), Ni; (■), LaCO$_3$OH; (▲), La(OH)$_3$.
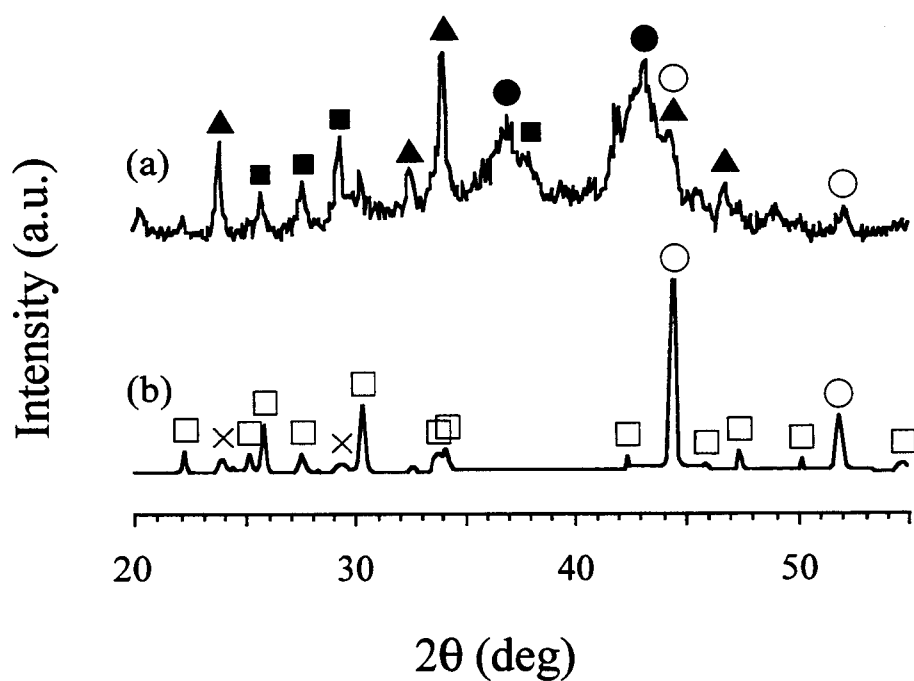
Figure 3.1.3. XRD patterns for Ni_5LaO_x, (a) just after pretreatment, (b) after reaction at 350 °C. ($\bullet$), NiO; ($\blacktriangle$), La_2NiO_4; ($\blacksquare$); La_2O_3; (O), Ni; ($\square$), $La_2O_2CO_3$; ($\times$), $LaCO_3OH$.

supposed to transform into La_2O_3, however, the peaks were not found in the XRD patterns while peaks for $La(OH)_3$ (Figure 3.1.2e; solid triangles) and $LaCO_3OH$ (solid squares) were clearly observed [22]. No peaks attributed to nickel carbide were recorded.

Peaks attributed to NiO (Figure 3.1.3a; solid circles) [22], La_2O_3 (solid squares) [22], and La_2NiO_4 (solid triangles) [18] were recorded in the XRD pattern of Ni_5LaO_x just after the pretreatment with hydrogen while the peaks of metallic nickel (open circles) were also observed. The peaks of the oxides disappeared and the intensity of the peaks for metallic nickel significantly increased in the pattern for the sample taken out from the reactor after the reaction at 350 °C (Figure 3.1.3b). The peaks attributed to $La_2O_2CO_3$ (squares) and $LaCO_3OH$ (crosses) were also seen in the pattern [22]. Only peaks attributed to metallic nickel were observed with Ni powder stabilized after the reaction at 350 °C (not shown). The crystallite sizes of metallic nickel for Ni_5LaO_x and Ni powder after the reaction were estimated as 29 and 35 nm, respectively.

Surface analyses by XPS

In order to clarify the source of the high activity of $LaNi_5$ at 250 °C, XPS analyses were performed with the catalysts after the reactions at 250 °C. The spectra for $Ni(2p_{3/2})$ were deconvoluted into two Gaussian peaks and the peak at 852.7-852.8 eV was attributed to metallic nickel while the broad peak at 854.8-855.3 eV was attributed to Ni^{2+} (Figure 3.1.4) [21]. The peak width and the intensity of the broad peak increased with an increase in the time-period of the reaction. The profiles for $O(1s)$ were also separated into two Gaussian peaks at 531.7-532.2 eV and 529.3-529.6 eV (Figure 3.1.5). The peak position of $La(3d_{5/2})$ was at 835.4 eV for the sample after the reaction for 6.5 h while that was at 834.7 eV just after the pretreatment with hydrogen (not shown). Since the binding
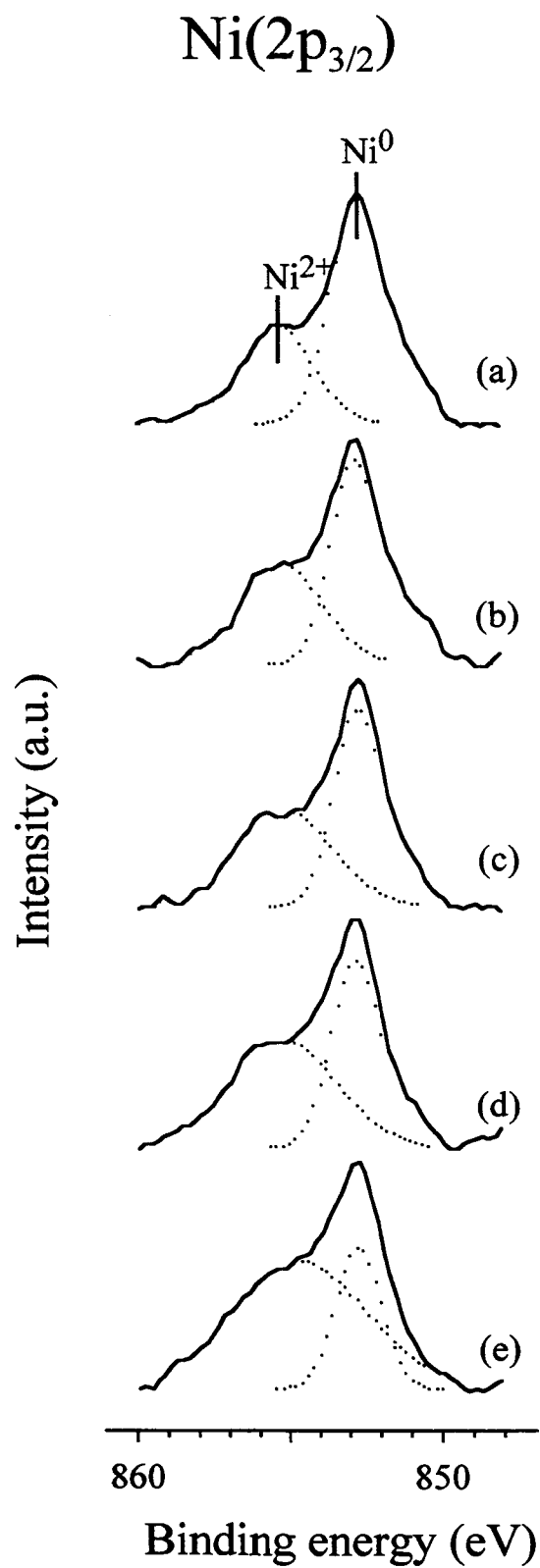
Ni(2p$_{3/2}$)

Figure 3.1.4. XPS spectra of Ni(2p$_{3/2}$) for LaNi$_5$, (a) just after pretreatment, (b) after reaction for 0.5 h, (c) 2 h, (d) 4 h, (e) 6.5 h.

O(1s)
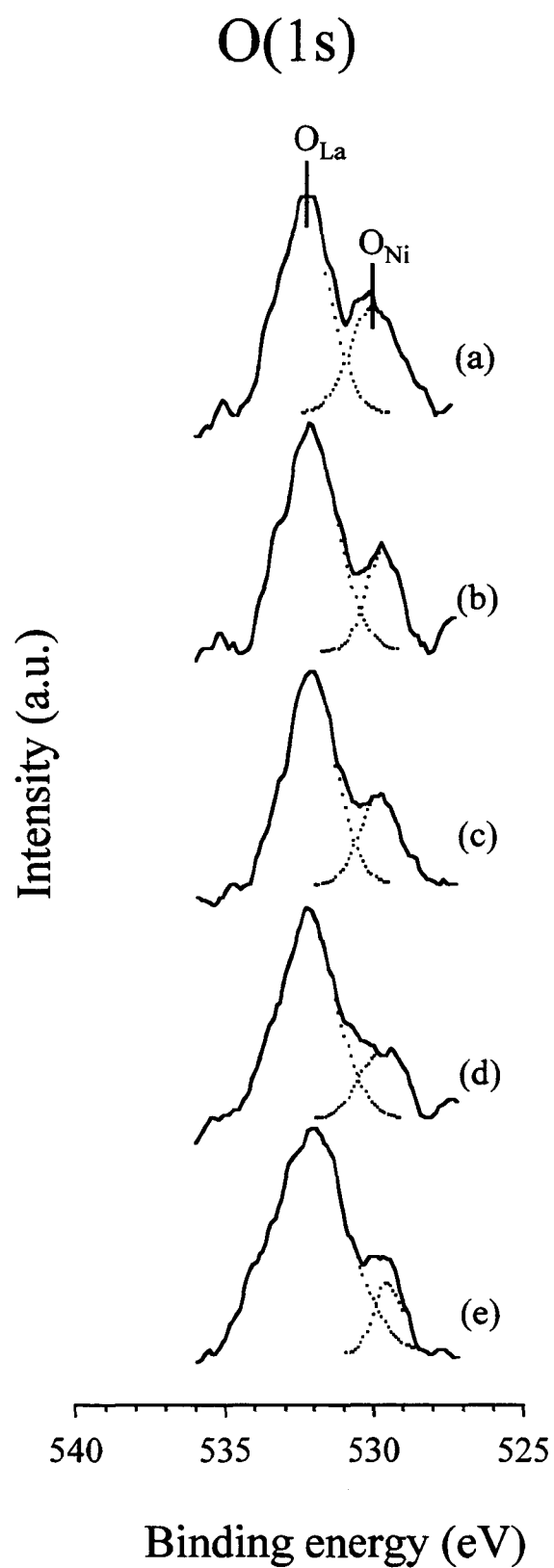
Figure 3.1.5. XPS spectra of O(1s) for LaNi$_5$, (a) just after pretreatment, (b) after reaction for 0.5 h, (c) 2 h, (d) 4 h, (e) 6.5 h.

energy of La(3d$_{5/2}$) for La$_2$O$_3$ was reported to be 834.9 eV [21], La^{3+} species were dominant on the surface of LaNi$_5$. The surface atomic ratio was calculated assuming that the atomic sensitivity factors of Ni(2p$_{3/2}$), La(3d$_{5/2}$), and O(1s) are 13.92, 26.50, and 2.85, respectively (see Table 3.1.2) [21]. A peak at 289 eV attributed to carbonate species was recorded in the spectra for C(1s) while no peak attributed to carbide species usually at 281-283 eV was recorded (not shown).

3.1.4. Discussion

The catalytic activity of LaNi$_5$ increases gradually during the reaction at 250 °C (see Figure 3.1.1). Although crystallites of metallic nickel appear clearly after the reaction for 2 h at 250 °C (see Figure 3.1.2c), the catalytic activity at 2 h-on-stream is not so high as that at 4 or 6.5 h-on-stream. The XRD pattern for Ni$_5$LaO$_x$ after the reaction also shows the presence of metallic nickel in the catalyst (see Figure 3.1.3b), however, the catalytic activity at 250 °C is not high. Hence, the formation of the metal crystallites in LaNi$_5$ does not account for the increase in the activity during the reaction at 250 °C, and it shows the formation of new active sites in LaNi$_5$.

The typical structure of intermetallic compound of LaNi$_5$ is destroyed and the phase was separated into nickel metal and La^{3+} compounds during the reaction (see Figure 3.1.2). Although no peaks attributed to nickel oxide or carbonate are present in the XRD patterns for LaNi$_5$, the result of XPS analyses shows presence of Ni^{2+} species on the surface. The binding energy of O(1s) at 529.3-529.6 eV (see Table 3.1.2) is close to that for NiO [21], suggesting presence of nickel oxide on the surface. It would be possible that nickel is oxidized in air after taken out from the reactor. However, the surface concentration of Ni^{2+} species increases with an increase in the time-on-stream and the position of the peak for Ni^{2+} shifted to a lower binding energy while the

Table 3.1.2. XPS analyses for LaNi$_5$.

Time-on-stream (h)	Binding energy / eV (Surface composition / mol%)					Atomic ratio	
	Ni^0	Ni^{2+}	O$_{Ni}$	O$_{La}$	La(3d$_{5/2}$)	O$_{Ni}$/Ni^{2+}	O$_{La}$/La
0	852.7(17.5)	855.3(12.3)	529.3(16.2)	531.7(35.4)	834.7(18.7)	1.3	1.9
0.5	852.7(15.5)	855.3(13.7)	529.3(12.8)	531.8(39.0)	834.9(19.1)	0.9	2.0
2	852.7(13.7)	855.2(14.1)	529.5(13.0)	531.8(40.9)	835.1(18.3)	0.9	2.2
4	852.7(11.0)	855.0(14.7)	529.6(12.0)	532.2(48.4)	835.5(14.0)	0.8	3.5
6.5	852.8(7.0)	854.8(19.4)	529.5(10.9)	532.2(48.0)	835.4(14.6)	0.6	3.3

ratio of O_{Ni}/Ni^{2+} decreases (see Figure 3.1.4 and Table 3.1.2). Hence, new nickel species other than nickel oxide are believed to be formed on the surface during the reaction.

Since the catalytic activity at 250 °C seems to depend on the surface concentration of Ni^{2+} (cf. Figure 3.1.1 and Table 3.1.2), we may infer that the new nickel species is the source of the increase in the activity. In the case of Ni_5LaO_x, the increase in the activity during the reaction is not so large as that of $LaNi_5$. In the former solid, $La_2O_2CO_3$ is mainly formed during the reaction and $La(OH)_3$ is not present (see Figure 3.1.3b). On the other hand, $La(OH)_3$ and $LaCO_3OH$ are formed in $LaNi_5$ during the reaction (see Figure 3.1.2), and it is supposed that the phase change of $LaNi_5$ is caused by water produced in the reaction.

Table 3.1.3. Lanthanum compounds formed after the reaction.

Catalyst	$La(OH)_3$	$LaCO_3OH$	$La_2O_2CO_3$
$LaNi_5$	+++++	+++	-
Ni_5LaO_x	-	++	+++

Note: Based on the peak intensity of XRD pattern.

The binding energy of O(1s) for lanthanum oxide was 529.5 eV (our result), and the major peaks of O(1s) for $LaNi_5$ are at 531.7-532.2 eV. Since the binding energy of O(1s) for metal hydroxide seems to be higher than that for metal oxide [21] and the energy for lanthanum carbonate was 532.0 eV (our result), the peaks can be attributed mainly to both the hydroxyl and carbonate species. Supposing that the surface hydroxyl groups are reactive to nickel under the reaction conditions, formation of the bonding such as Ni-O-La will take place and it can account for the formation of the new nickel species on the

47

surface. The XRD pattern of Ni_5LaO_x after the reaction shows discernible formation of $LaCO_3OH$ and it may result in the gradual increase in the catalytic activity by formation of the new nickel species (see Table 3.1.3). Formation of other active species such as carbide during the reaction would be possible [19, 23], however, no presence of the species was evidenced in this study while further investigation is necessary to clarify the details.

3.1.5. References

[1]   R. S. Craig, W. E. Wallace and H. Kevin Smith, in E. C. Subbarao and W. E. Wallace (eds.), *Science and Technology of Rare Earth Materials*, Academic Press, New York, 1980.

[2]   K. Soga, H. Imamura and S. Ikeda, *Nippon Kagaku Kaishi*, 9(1977)1299.

[3]   K. Soga, H. Imamura and S. Ikeda, *Nippon Kagaku Kaishi*, 7(1978)923.

[4]   K. Soga, T. Sano, H. Imamura, M. Sato and S. Ikeda, *Nippon Kagaku Kaishi*, 7(1978)930.

[5]   K. Soga, T. Sano, M. Sato and S. Ikeda, *Nippon Kagaku Kaishi*, 5(1979)573.

[6]   J. R. Johnson, Z. Gavra, P. Chyou and J. J. Reilly, *J. Catal.*, 137(1992)102.

[7]   A. Elattar, T. Takeshita, W. E. Wallace and R. S. Craig, *Science*, 196(1977)1093.

[8]   Gary B. Atkinson and Larry J. Nicks, *J. Catal.*, 46(1977)417.

[9]   C. A. Luengo, A. L. Cabrera, H. B. MacKay and M. B. Maple, *J. Catal.*, 47(1977)1.

[10]   H. Imamura and W. E. Wallace, *Am. Chem. Soc., Div. Fuel Chem.*, 25(1979)82.

[11]   W. E. Wallace, A. Elattar, H. Imamura, R. S. Craig and A. G. Moldovan, in E. C. Subbarao and W. E. Wallace (eds.), *Science and Technology of Rare Earth Materials*, Academic Press, New York, 1980.

[12]   S. Kasaoka, E. Sasaoka and J. Misumi, *Nippon Kagaku Kaishi*, 7(1982)1246.

[13]   J. Barrault and D. Duprez, *J. Less-Common Met.*, 89(1983)537.

[14]   J. Muller, V. Pour and A. Regner, *J. Catal.*, 11(1968)326.

[15]   V. Pour, *Collect. Czech. Chem. Commun.*, 35(1970)2203.

[16]   T. Inui, M. Funabiki, M. Suehiro and T. Sezume, *J. Chem. Soc., Faraday Trans.*, 75(1978)787.

[17]   T. Inui, M. Funabiki and Y. Takegami, *Ind. Eng. Chem. Prod. Res. Dev.*, 19(1980)385.

[18]   E. Ruckenstein and Y. H. Hu, *J. Catal.*, 161(1996)55.

[19]   J. Barrault, A. Guilleminot, J. C. Achard, V. Paul-Boncour, A. Percheron-Guegan, L. Hilaire and M. Coulon, *Appl. Catal.*, 22(1986)273.

[20]   H. P. Klug and L. E. Alexander, in *X-ray Diffraction Procedures*, John Wiley and Sons Inc., New York, 1954.

[21]   C. D. Wagner, W. M. Riggs, L. E. Davis, J. F. Moulder, in G. E. Muilenberg (ed.), *Handbook of X-ray photoelectron spectroscopy*, Perkin-Elmer Corp., Minnesota, 1978.

[22]   JCPDS powder diffraction files:4-835(NiO);4-850(Ni);17-126(LaNi$_5$); 24-554(La$_2$O$_3$);26-815(LaCO$_3$OH);36-1481(La(OH)$_3$);37-804(La$_2$O$_2$CO$_3$).

[23]   Z. L. Wang, C. Colliex, V. Paul-Boncour, A. Percheron-Guegan, J. C. Achard and J. Barrault, *J. Catal.*, 105(1987)120.

3.2. Comparative study of the hydrogenation of CO_x over Fe catalyst

3.2.1. Introduction

Iron-based catalysts are usually employed in hydrogenation of CO to hydrocarbons and oxygenated products (Fischer-Tropsch synthesis) [1-9]. The active phase of the reaction is believed to be iron carbide species, while contribution of other phases such as metallic iron has yet to be clear. Miller and Moskovits showed different pathway for formation of oxygenates and it implies presence of other active phases [10]. However, identification of the active phase is not easy because the surface of iron is not stable during the reaction. That is, formation of carbide species accompanies accumulation of carbon on the surface and in case of Fe_2O_3, which is often used as a catalyst precursor, reduction of the oxide to Fe_3O_4 and metallic iron also proceed [5].

Iron catalysts are also active to hydrogenation of CO_2 [11-15]. The hydrogenation can be understood sequential reaction of reduction of CO_2 to CO and hydrogenation of CO. However, some dissimilarity from CO hydrogenation was reported [16]. Dwyer and Somorjai compared the reactions from CO and CO_2 over iron foil and they showed less hydrocarbon-chain growth and higher specific methanation rate in CO_2 hydrogenation [9].

In this section we have compared the activation process in hydrogenation of CO and CO_2 over iron catalysts in order to avoid excessive carbide formation which proceeds in the reaction for long period and have characterized the active sites of the reactions with CO and CO_2 which is always by-produced in the Fischer-Tropsch reaction.

3.2.2. Experimental

Iron oxide was prepared by precipitation from an aqueous solution of $Fe(NO_3)_3$ (1 M) with NH_4OH (1 M) at 70 °C. After being stirred at room temperature for 12 h, the precipitate was filtrated, dried at 120 °C for 6 h, and

calcined in air at 500 °C for 5 h. The resulting solid was crashed into granules less than 60 mesh.

The hydrogenation of carbon oxides was carried out with a fixed-bed flow reactor made of stainless steel tube with 10-mm i.d. A catalyst was pretreated with a hydrogen stream (10 vol%) diluted with nitrogen under atmospheric pressure at 350 °C or 500 °C for 12 h. After introduction of a reactant mixture (33% CO in H_2 or 25% CO_2 in H_2) at room temperature the pressure was raised to 1 MPa and temperature was set at 250 °C. The effluent gas was analyzed with on-line gas chromatographs of which columns were Porapak Q for CO_2, MS-13X for methane and CO, PLOT column (Fused Silica, Al_2O_3/KCl) for hydrocarbons, and PEG-6000(15%)+TCEP(8%) supported on Chromosorb WAW(60/80 mesh) for alcohols. Yields and selectivities were calculated on the basis of carbon numbers in the products.

The BET surface areas of the catalysts were determined from the isotherms of nitrogen physisorption. X-ray diffraction (XRD) patterns were recorded with a Rigaku ROTAFLEX diffractometer (Cu-Kα). The mean crystallite size of the catalyst was estimated from the peak width using the equation of Scherrer [17]. Surface analyses by X-ray photoelectron spectroscopy (XPS) were performed with a Shimadzu ESCA-750. The spectra were recorded after argon-ion sputtering for 1 min (2 kV, 25 mA). The binding energy was corrected with the energy of C(1s) (284.6 eV) for carbon contaminant [18].

3.2.3. Results

Hydrogenation of CO

Hydrogenation of CO was carried out over iron catalyst reduced at 500 °C. Conversion of CO increased in the initial stage of the reaction and it was mostly stabilized after 5 h-on-stream (Figure 3.2.1, solid symbols). The major
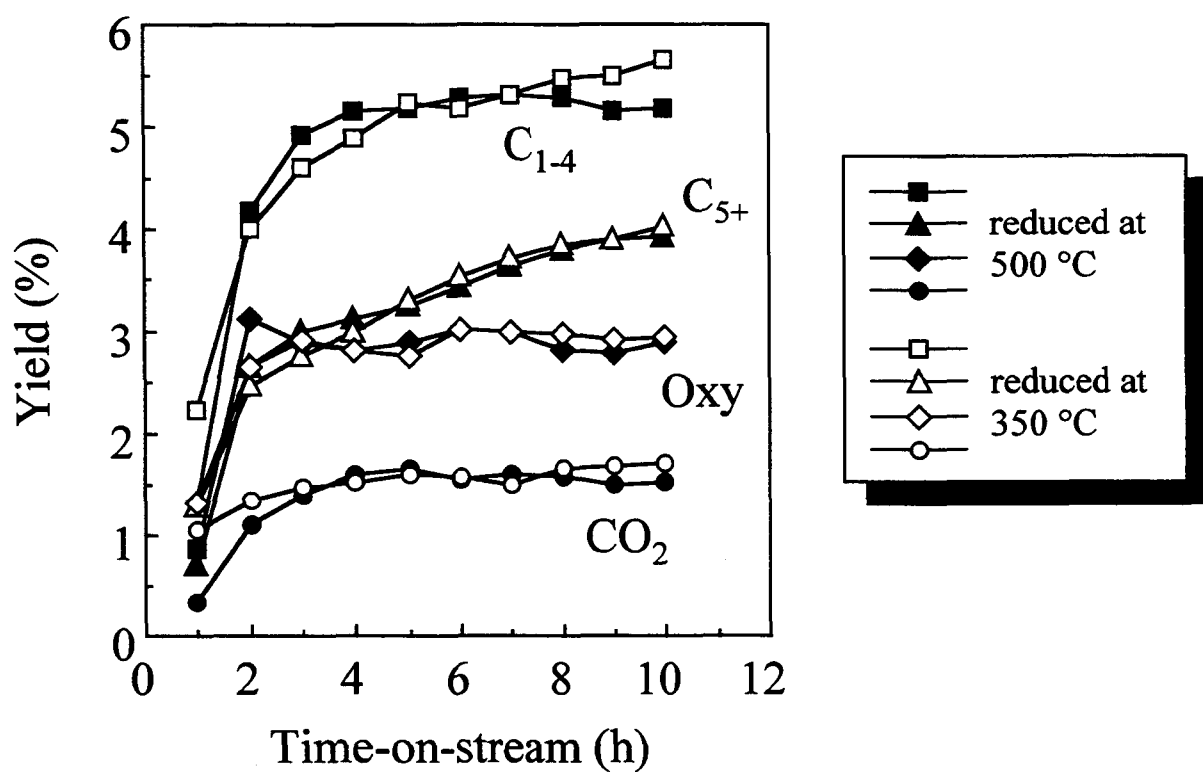
Figure 3.2.1. Hydrogenation of CO at 250 °C over iron catalyst. Open symbols, reduced at 350 °C; solid symbols, reduced at 500 °C. F/W, 9,000 ml g^{-1} h^{-1}.
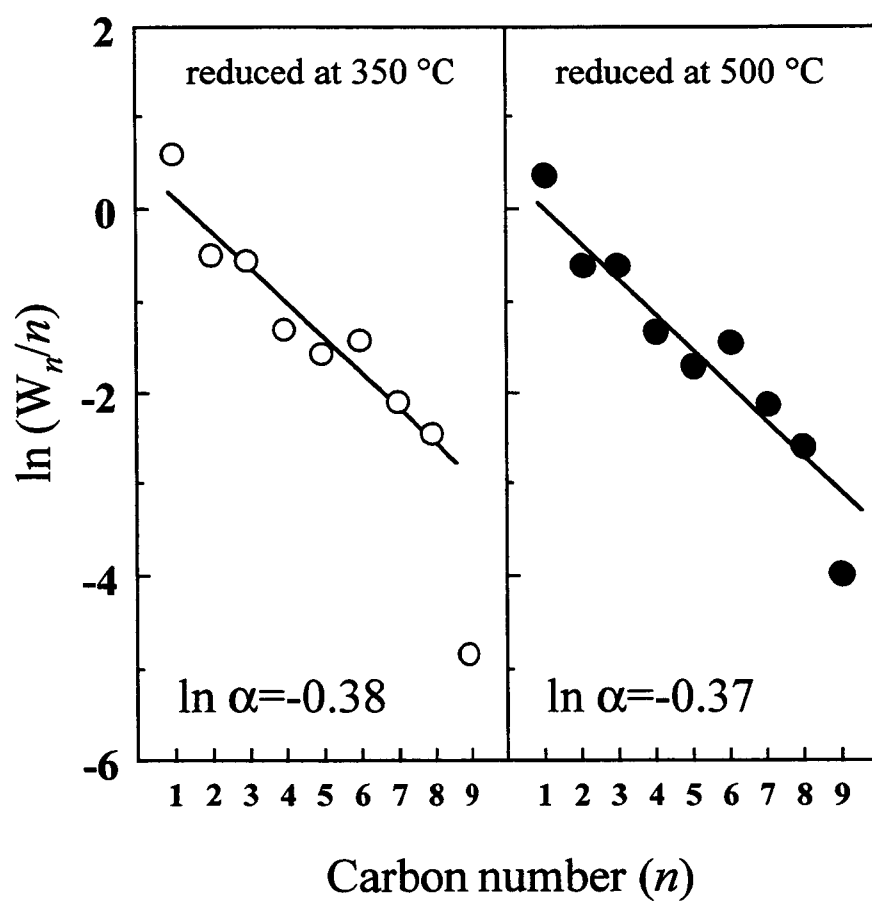
Figure 3.2.2. Schulz-Flory plots for the hydrogenation of CO over iron catalyst. Open symbols, reduced at 350 °C; solid symbols, reduced at 500 °C.

Table 3.2.1. Catalytic activity of Fe catalyst on the olefin content and the yield of alcohols with different reduction temperatures.

Reactant (F/W)[a]	Reduction Temp.(°C)	CO_x Conv. (%)	olefin/(olefin+paraffin)			Yield(%)			BET surface area (m² g⁻¹)[b]
			C_2	C_3	C_4	MeOH	EtOH	PrOH	
CO/H_2 (9,000)	500	13.5	0.259	0.668	0.661	1.68	0.86	0.33	1.8
CO/H_2 (9,000)	350	10.2	0.176	0.564	0.574	1.67	0.92	0.35	1.5
CO_2/H_2 (1,200)	500	14.3	0.010	0.029	0.028	1.18	0.19	- [c]	2.2
CO_2/H_2 (1,200)	350	9.5	0.012	0.048	0.060	1.13	0.15	- [c]	2.1

Conditions: temperature, 250 °C; pressure, 1 MPa; time-on-stream, 10 h.

[a] ml g-cat⁻¹ h⁻¹.

[b] after reaction.

[c] not detected.

products were C_1-C_9 hydrocarbons, C_1-C_3 alcohols, and CO_2. Over the catalyst reduced at 350 °C the catalyst was activated sooner than that pretreated at 500 °C while the activities after the activation process were very similar (Figure 3.2.1, open symbols).

In general, waxes and other heavy products formed in the reaction accumulate in catalyst pores, and it rather deactivates the catalyst [2]. Under the present reaction conditions few heavy products were detected and no significant deactivation was observed after 10 h-on-stream while the mass balance was always more than 95%. The BET surface areas were 3.5 and 4.5 m^2 g^{-1} for the samples just after the reduction at 500 °C and 350 °C, respectively, and they decreased to 1.8 and 1.5 m^2 g^{-1}, respectively, after the reaction (Table 3.2.1).

The product distributions of hydrocarbons after 10 h-on-stream mostly obeyed the Schulz-Flory's law as shown in Figure 3.2.2. From the slope of the plots the logarithms of probability of chain growth, ln α, were obtained as -0.38 and -0.37 for the catalysts reduced at 350 and 500 °C, respectively. The catalyst reduced at 350 °C produced appreciably lower selectivities to olefins (C_{2-4}) than that reduced at 500 °C (see Table 3.2.1). No significant difference was observed in the yields of alcohols between these catalysts.

Hydrogenation of CO_2

When CO_2 was a reactant the activation process was slow and the catalytic activity still increased with time-on-stream even after 5 h (Figure 3.2.3). The space-time-yield was significantly low compared with the CO hydrogenation, e.g., the values for methane at 10 h-on-stream were 0.4 mmol g^{-1} h^{-1} and 2 mmol g^{-1} h^{-1} for CO_2 and CO conversions over the catalyst reduced at 500 °C, respectively. After 1 h-on-stream the activity of the catalyst reduced at 350 °C was very small while no obvious difference in activity was present
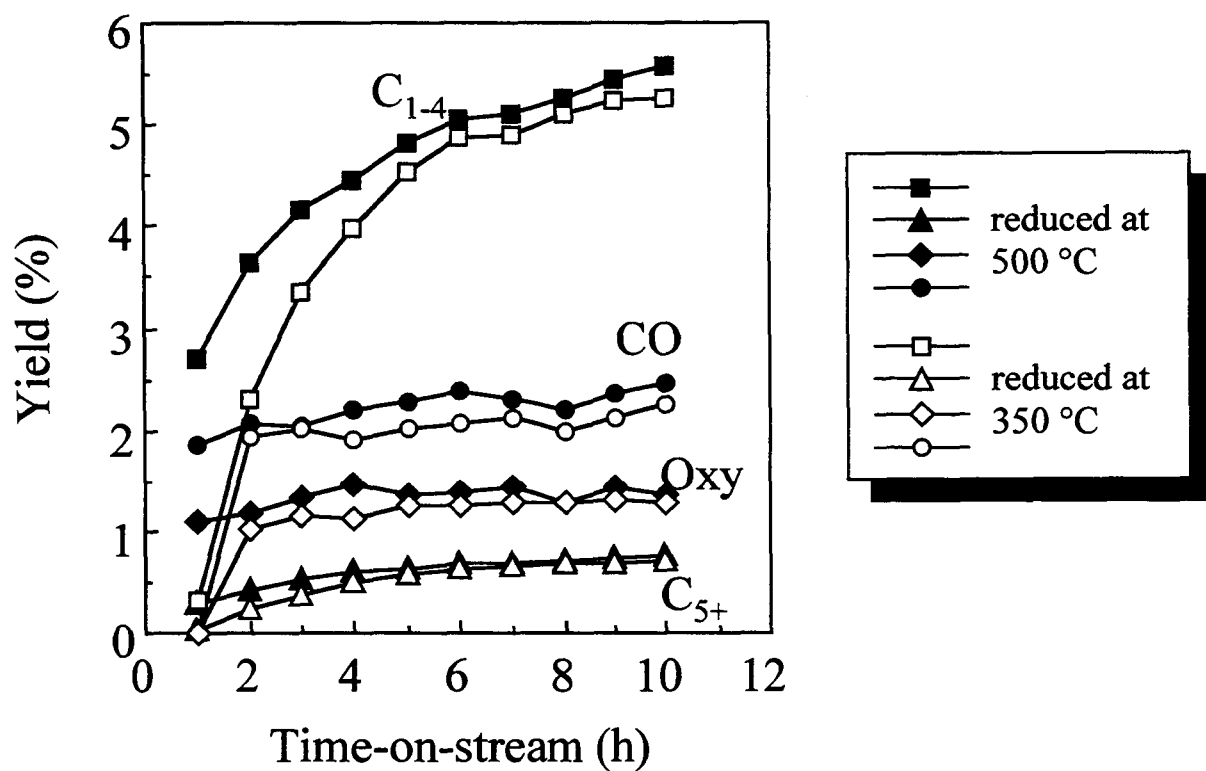
Figure 3.2.3. Hydrogenation of CO_2 at 250 °C over iron catalyst. Open symbols, reduced at 350 °C; solid symbols, reduced at 500 °C. F/W, 1,200 ml g-cat^{-1} h^{-1}.
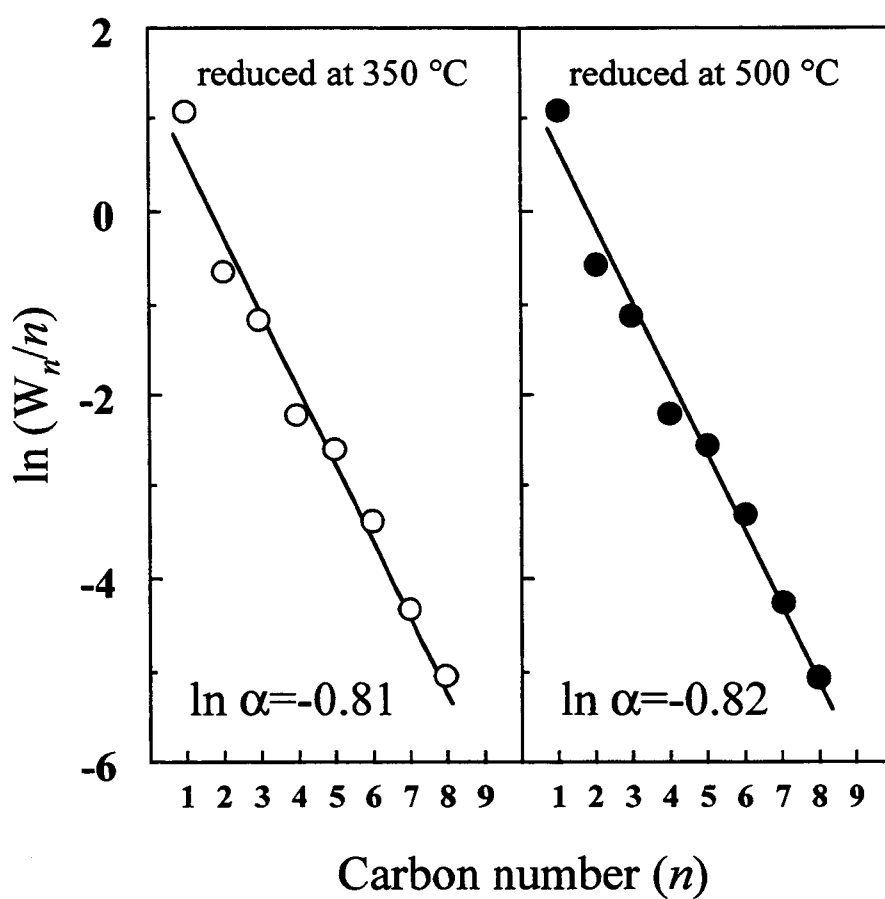
Figure 3.2.4. Schulz-Flory plots for the hydrogenation of CO_2 over iron catalyst: open symbols, reduced at 350 °C; solid symbols, reduced at 500 °C.

between the catalysts pretreated at 350 and 500 °C after 10 h-on-stream. The selectivities to olefins were very small and methanol was mainly produced as oxygenate (see Table 3.2.1). The distribution of hydrocarbons was also followed by the Schulz-Flory's law but the values of ln α were -0.81 and -0.82 for the catalysts reduced at 350 and 500 °C, respectively (Figure 3.2.4).

XRD measurements

X-ray diffraction (XRD) analyses were performed with the iron catalysts. A clear peak at 44.5° attributed to α-Fe was found for the catalyst taken out from the reactor just after the pre-reduction at 500 °C while a slight peak attributed to Fe_3O_4 was also present at 35.3° in 2θ (Figure 3.2.5a) [19]. The mean crystallite size of α-Fe in the sample just after the pretreatment was estimated as 65 nm from the XRD peak at 44.5°. The catalyst taken out from the reactor after the reaction with CO kept the structure of α-Fe and small peaks attributed to χ-$Fe_{2.2}C$ were also found (Figure 3.2.5b) [3]. No significant change in the crystallite size of α-Fe was detected. After CO_2 hydrogenation a very slight peak at 41.8° was recorded with a main peak attributed to α-Fe (Figure 3.2.5c). The peaks attributed to α-Fe and Fe_3O_4 were seen in the pattern of catalysts just after reduced at 350 °C (Figure 3.2.5d) The peaks of χ-$Fe_{2.2}C$ were also recorded with the sample reduced at 350 °C after the reaction with CO (Figure 3.2.5e). On the other hand only peaks attributed to Fe_3O_4 were recorded after the reaction with CO_2 (Figure 3.2.5f).

In the cases of the catalysts used in CO_2 hydrogenation no peaks attributed to the carbide species nor metallic iron phase were recorded (Figures 3.2.5e and f). No significant change in the structure was detected for the catalysts reduced at 350 or 500 °C.
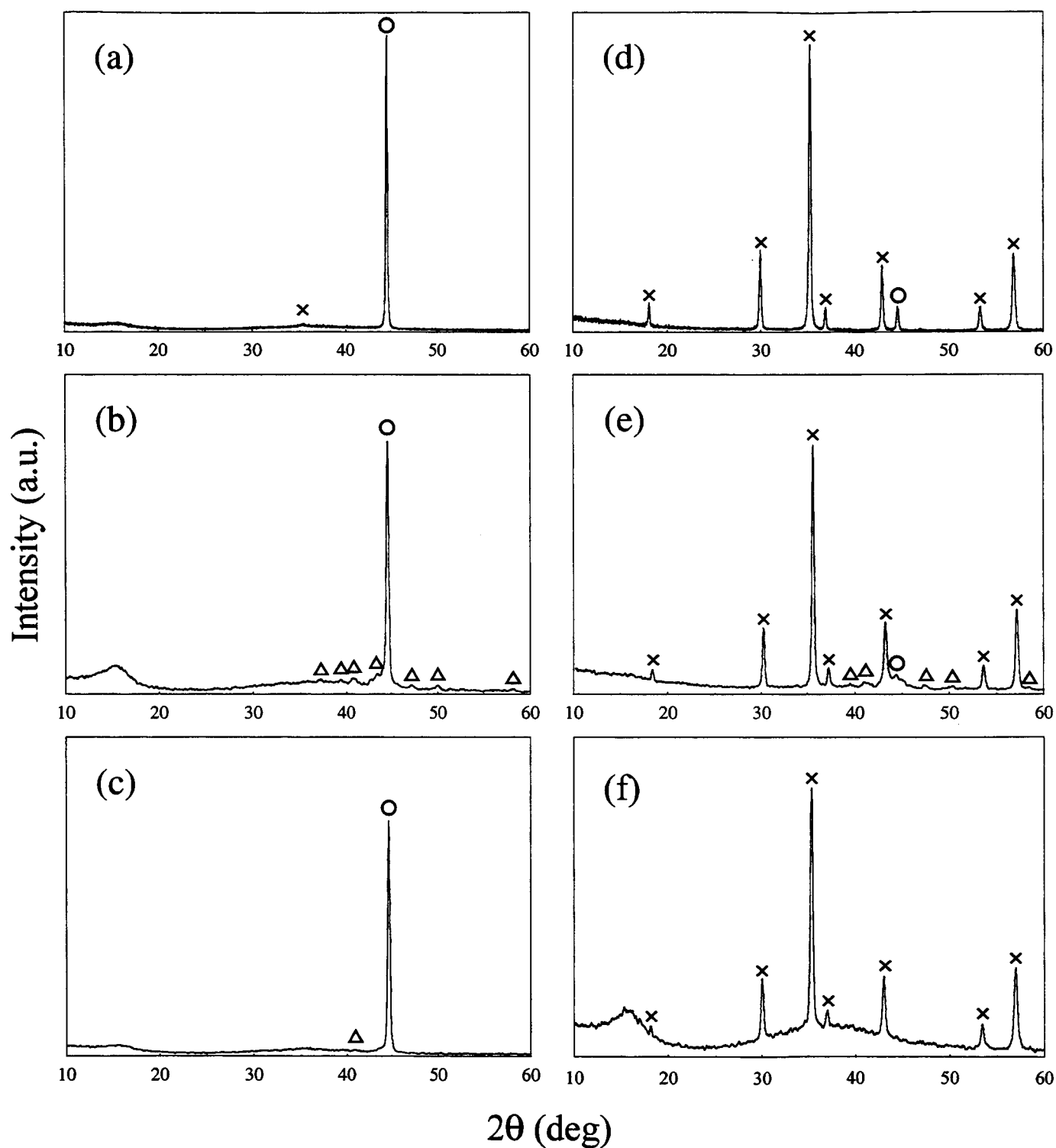
Figure 3.2.5. XRD patterns for iron catalysts: (O)Fe; (X)Fe_3O_4; ($\triangle$)$Fe_{2.2}C$: (a) just after reduction at 500 °C; (b) followed by reaction with CO; (c) followed by reaction with CO_2; (d) just after reduction at 350 °C; (e) followed by reaction with CO; (f) followed by reaction with CO_2.

59

Surface analyses by XPS

Although the XRD analyses did not show clear change in the structure of the catalyst except formation of carbide species during the hydrogenation of CO, change in the oxidation state of the surface iron was detected by recording XPS of the catalysts. The sample was taken out from the reactor and transferred into XPS instrument in air, but it was confirmed that the exposure of samples to air is not a serious drawback for the reliability of the characterization of the catalyst [5, 20]. In the range of Fe ($2p_{3/2}$) a major peak attributed to Fe[0] was recorded at 706.9 eV in the XPS for the catalyst just after the reduction at 500 °C (Figure 3.2.6a) [18]. The spectrum can be deconvoluted to three Gaussian peaks and minor peaks were at 709.5 and 712.6 eV. The former can be attributed to Fe^{2+} and the latter to Fe^{3+} [18]. After the reaction with CO the peak at 706.9 eV was intensified (Figure 3.2.6b) but in the case of the reaction with CO_2 the peak became small and both the peaks at 709.5 and 712.6 eV were mainly present (Figure 3.2.6c).

After the reduction at 350 °C the peak at 706.9 eV was not recorded (Figure 3.2.6d) but a small peak at 706.9 eV attributed to metallic species was seen in the XPS after the following reaction with CO (Figure 3.2.6e). The XPS profile after the reaction with CO_2 was similar to that just after the pretreatment at 350 °C (Figure 3.2.6f).

3.2.4. Discussion

In the reactions with CO no significant change in the activity can be seen with the iron catalysts pretreated at different temperatures except in the initial stage of the reaction (see Figure 3.2.1). Dictor and Bell reported that Fe_2O_3 is slowly activated in the initial stage of the Fischer-Tropsch synthesis [3], but in the case of the catalyst reduced at 350 °C, of which major structure is Fe_3O_4, the activation process is rather quick compared with that pretreated at 500 °C.
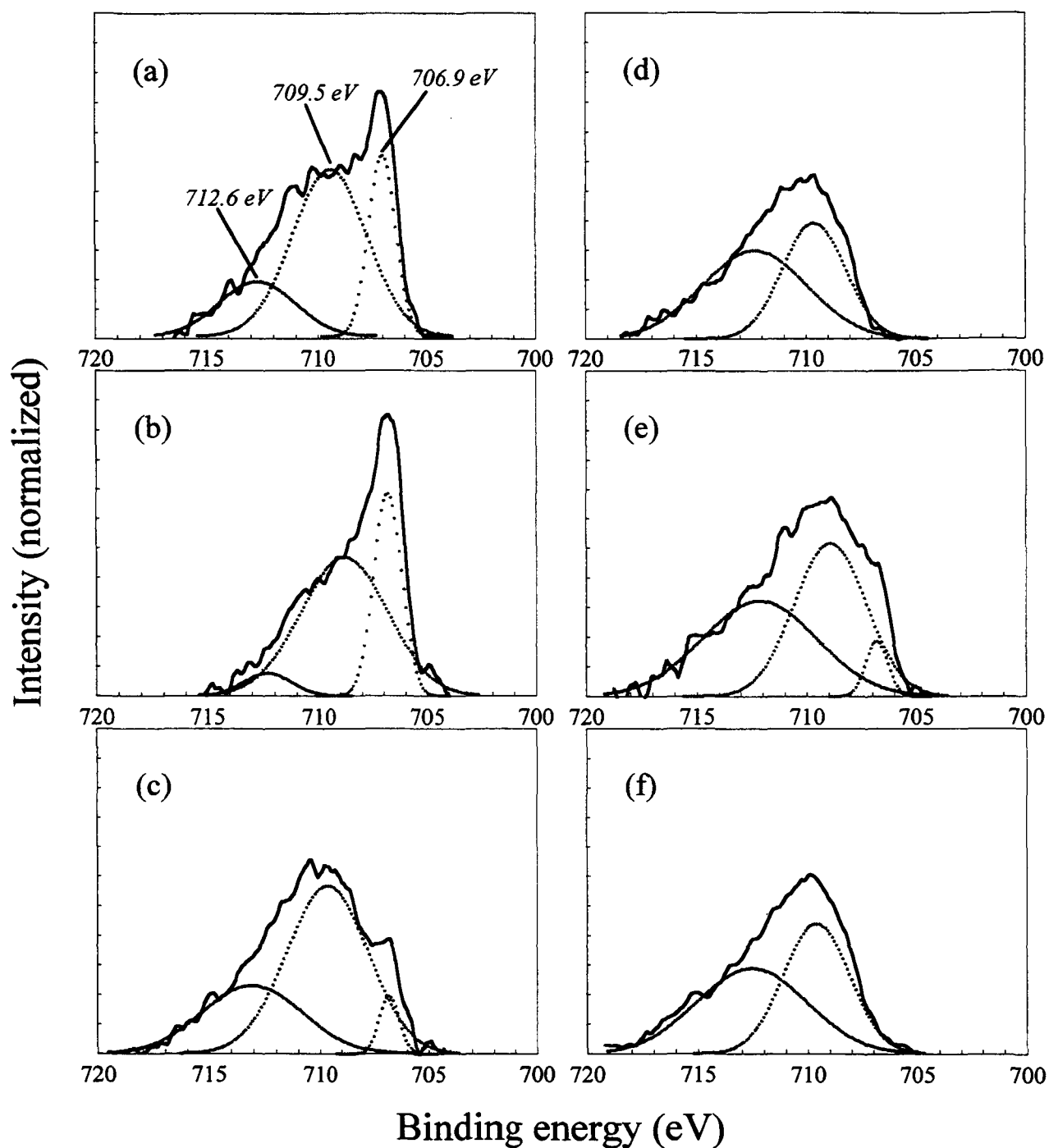
Figure 3.2.6. XPS spectra of Fe($2p_{3/2}$) for iron catalysts: (a) just after reduction at 500 °C; (b) followed by reaction with CO; (c) followed by reaction with CO_2; (d) just after reduction at 350 °C; (e) followed by reaction with CO; (f) followed by reaction with CO_2.

Reymond et al. showed formation of χ-Fe$_{2.2}$C accompanied with the reduction of Fe$_2$O$_3$ to Fe$_3$O$_4$ during the reaction [5]. It is general understanding that iron carbides on the surface are active species of Fischer-Tropsch reaction, and the carbide species can be observed in the XRD pattern of both the used iron catalysts reduced at 350 °C and at 500 °C. Hence, Fe$_3$O$_4$ is an active precursor as well as metallic iron while inactive carbide is often formed on the metal [5].

Iron is known as the catalyst for the water gas shift (WGS) reaction. In order to evaluate the contribution of the WGS reaction to CO hydrogenation, the value of Kp (equilibrium constant for WGS reaction) is introduced as follows (eq. 3.2.1);

$$K p = \frac{P_{(CO_2)}P_{(H_2)}}{P_{(CO)}P_{(H_2O)}}$$
(3.2.1)

, where P(i) represents a partial pressure of a component i. The partial pressure of each component was estimated from the product distribution. The theoretical value of Kp at 250 °C is 56 and both the values of Kp for the CO hydrogenation over the catalysts reduced at 350 °C and 500 °C after 10 h-on-stream were only 0.4. On the other hand, a reverse WGS reaction takes place in the CO$_2$ hydrogenation and the values of 1/Kp for the reaction over the catalysts reduced at 350 °C and 500 °C were calculated as 0.1-0.2 $\times 10^{-2}$, while the equilibrium value is 1.8$\times 10^{-2}$. This suggests that the formation rate of CO is fairly small under the reaction conditions.

Although Dewyer and Somorjai reported a higher methanation rate from CO$_2$ and H$_2$ over iron foils than that from CO and H$_2$ at 300 °C [9], the formation rate of hydrocarbons from CO$_2$ in our study was significantly lower than that from CO partly because of the low formation rate of CO under the reaction conditions. The surface oxidation state of the catalyst reduced at 500 °C after

the reaction with CO_2 is similar to that for the catalyst reduced at 350 °C after the reaction with CO (cf. Figures 3.2.6c and e). However, the product distribution of the reaction with CO_2 is significantly different from that for the reaction with CO, appearing that the surface oxidation state does not seriously affect to the nature of the active sites. Accumulation of carbon and oxygen was observed over iron foil in the reaction with CO_2 [9], suggesting that active carbide species is formed on the surface. Hence, formation of carbide and oxide probably occurs on the metallic surface of the iron catalyst reduced at 500 °C during the activation process in the reaction with CO_2. The very slight peak at 41.8° may be attributed to $\chi\text{-Fe}_{2.2}C$, suggesting presence of the carbide species. In presence of CO_2 elimination of carbide readily takes place to form CO and it will suppress the formation of the active carbide species. Consequently, the surface concentration of carbide species is lower in the case of the reaction with CO_2. It is reasonable that the lower concentration of the active sites results in small probability of chain growth and increasing in the chance of hydrogenation. Although carbide species can be formed readily on the surface of Fe_3O_4, the activation of the catalyst reduced at 350 °C was slow. The XPS analyses show that the surface of the catalyst is oxidized after the reaction, suggesting that the surface is close to that of Fe_2O_3 whose activation is very gradual [3].

3.2.5. References

[1]   S. Soled, E. Iglesia, R. A. Fiato, *Catal. Lett.*, 7(1990)271.

[2]   D. B. Bukur, D. Mukesh, S. A. Patel, *Ind. Eng. Chem. Res.*, 29(1990)194.

[3]   R. A. Dictor, A. T. Bell, *J. Catal.*, 97(1986)121.

[4]   M. E. Dry, in: J. R. Anderson and M. Boudart (Eds.), Catalysis Science and Technology, vol. 1, Springer, New York, (1982)159.

[5]   J. P. Reymond, P. Mériaudeau, S. J. Teichner, *J. Catal.*, 75(1982)39.

[6]   F. Blanchard, J. P. Reymond, B. Pommier, S. J. Teichner, *J. Mol. Catal.*, 17(1982)171.

[7]   R. J. Madon, W. F. Taylor, *J. Catal.*, 16(1981)32.

[8]   G. B. Raupp. W. N. Delgass, *J. Catal.*,58(1979)361.

[9]   D. J. Dwyer, G. A. Somorjai, *J. Catal.*,52(1978)291.

[10]   D. Miller, M. Moskovits, *J. Am. Chem. Soc.*,111(1989)9250.

[11]   H. Ando, Q. Xu, M. Fujiwara, Y. Matsumura, M. Tanaka, Y. Souma, *Catal. Today*,45(1998)229.

[12]   G. Kishan, M.-W. Lee, S.-S. Nam, M.-J. Choi, K.-W. Lee, *Catal. Lett.*, 56(1998)215.

[13]   P. H. Choi, K.-W. Jun, S.-J. Lee, M.-J. Choi, K.-W. Lee, *Catal. Lett.*, 40(1996)115.

[14]   J.-F. Lee, W.-S. Chern, M.-D. Lee, T.-Y. Dong, *Can. J. Chem. Eng.*, 70(1992)511.

[15]   M.-D. Lee, J.-F. Lee, C.-S. Chang, *Bull. Chem. Soc. Jpn.*,62(1989)2756.

[16]   M. Pijolat, V. Perrichon, M. Primet, P. Bussiére, *J. Mol. Catal.*, 17(1982)367.

[17]   H. P. Klug and L. E. Alexander, *X-ray Diffraction Procedures*, John Wiley and Sons Inc., New York, 1954.

[18]   C. D. Wagner, W. M. Riggs, L. E. Davis, J. F. Moulder, in G. E. Muilenberg (ed.), *Handbook of X-ray photoelectron spectroscopy*, Perkin-Elmer Corp., Minnesota, 1978.

[19]   JCPDS powder diffraction files: 6-696, 19-629

[20]   J. A. Amelse, J. B. Butt, L. H. Schwartz, *J. Phys. Chem.*,84(1980)3363.

Conclusions

The highly effective catalysts that can convert CO_2 into hydrocarbons were developed. The bulk and surface analyses have been performed in order to clarify the active species in the reactions of CO/H_2 and CO_2/H_2.

In chapter 1, the hydrogenation of CO_2 into methane using intermetallic compounds $LaNi_4X$ (X=Ni, Cr, Al, Cu) as catalyst precursors has been performed. It was shown that $LaNi_5$ and $LaNi_4Cr$ effectively catalyzed the methanation of CO_2. XRD patterns of these catalysts showed the formation of metallic nickel in the structure during the reaction. Aggregation of metallic nickel hardly took place in $LaNi_4Al$ and $LaNi_4Cu$ which were inactive at 250 °C. There is no correlation between the hydrogen storage ability and the catalytic activity. The presence of metallic nickel in the structure is essential for high catalytic activity to the conversion of CO_2, but at the same time, the presence of lanthanum in the solids could also be indispensable to high activity.

In chapter 2, the catalytic hydrogenation of CO_2 over Fe-Cu catalysts was carried out. In section 2.1, it was found that the surface density of sodium was not negligible in the catalysts containing sodium less than 0.1 wt% and that the major surface phases of the catalysts were FeO and/or $FeCO_3$ after reaction. The clear relationship was revealed between the surface basicity of the catalyst and the olefin content in the product. In section 2.2, hydrogenation of CO_2 over iron catalysts has been carried out and compared the activity obtained with CO. The rates of hydrocarbon and alcohol formation were higher in the reaction with CO. The rates of hydrocarbon and alcohol formation were suppressed by addition of steam to the reactant gas mixture of H_2/CO or H_2/CO_2. Although no significant change in the structure of the catalyst was observed by the XRD analyses, change in the oxidation state of the surface iron was detected by recording XPS of the catalysts. During the

65

reaction with CO, the catalyst surface was further reduced even after the reduction at 500 °C, while oxidized in the reaction with CO_2. Change in product distribution and the results of XPS analyses showed that the iron carbide is the active site for hydrocarbon formation and the oxygen species in iron hydroxide (O_{Fe-OH}) may be relevant to the formation of MeOH.

In chapter 3, characterization of the catalysts for the hydrogenation of CO_2 has been performed. In section 3.1, the hydrogenation of CO_2 to methane can be catalyzed over an intermetallic compound of $LaNi_5$ at 250-350 °C. The catalytic activity at 250 °C increases during the reaction while XRD analyses show that the structure of the compound decomposes to $La(OH)_3$, $LaCO_3OH$, and metallic nickel. Formation of metallic nickel species during the reaction also takes place in a nickel-lanthanum oxides catalyst prepared by a coprecipitation method. However, the activity is not so high as the former catalyst. Surface analyses by XPS suggest that new nickel species interacting with lanthanum cation, possibly Ni-O-La, are formed in $LaNi_5$ during the reaction, and the species are supposed to be rather active than metallic nickel. In section 3.2, when the major phase of the iron catalyst is Fe_3O_4, active carbide species are readily formed on the surface as well as on the metallic iron during the reaction with CO. Simultaneously, reduction of the surface oxide to metal takes place. On the other hand, oxidation of the surface iron proceeds during the reaction with CO_2, and a slight quantity of carbide species are formed on the surface. The formation of active carbide species may be suppressed in presence of CO_2 to give CO. Hence, the concentration of the active carbide species is lower in the reaction with CO_2 than in CO reaction, and the lower concentration results in (i) lower space time yield of hydrocarbons, (ii) higher selectivity to light hydrocarbons, and (iii) higher paraffin selectivity in the products.